Chemical Engineering Journal 513 (2025) 162749

Contents lists available at ScienceDirect

Chemical Engineering Journal

journal homepage: www.elsevier.com/locate/cej

Rapid formation of CO_2 hydrate with high storage capacity via a novel "self-siphoning" principle

Faping Liu [a], Yanhong Wang [a,*], Xuemei Lang [a,b], Gang Li [a], Shuanshi Fan [a,b,*]

[a] School of Chemistry and Chemical Engineering, South China University of Technology, Guangzhou 510640, China
[b] Key Laboratory of Fuel Cell Technology of Guangdong Province, Guangzhou 510640, China

ARTICLE INFO

Keywords:
CO_2 hydrate
CO_2 sequestration
Fulvic acid
Self-siphoning

ABSTRACT

Hydrate-based CO_2 sequestration has been recognized as an effective technology for long-term oceanic CO_2 sequestration to reduce CO_2 emissions and achieve carbon neutrality. However, the slow CO_2 hydrate formation rate has hindered the large-scale application of this technology. In this work, fulvic acid (FA) was employed to achieve rapid CO_2 hydrate formation from liquid CO_2 in seawater of the South China Sea in a high-pressure visual reactor, and CO_2 hydrate nucleation and growth were completed within 30.0 min. The average hydrate growth rate reached encouragingly high as 4.11 mmol CO_2/(mol H_2O·min). Compared with other additives reported to date, the average conversion rate of water to hydrate was the highest. A high CO_2 storage capacity of 121.8 V/V was obtained for 500 ppm FA. Liquid CO_2 could completely consume liquid water and convert it into hydrates within 30.0 min at 279.2 K. The addition of FA triggered the "self-siphoning" phenomenon that aqueous solution was quickly sucked into the hydrate pores. It leads to CO_2 hydrate formation being accelerated by 1 to 2 orders of magnitude and achieving high storage capacity, paving the way for large-scale oceanic CO_2 sequestration.

1. Introduction

Carbon dioxide (CO_2), as a major greenhouse gas, causes the greenhouse effect, resulting in environmental crises such as melting glaciers and rising sea levels [1,2]. Hydrate-based CO_2 sequestration has been considered as a potential means to effectively mitigate global warming and thus reduce atmospheric CO_2 emissions [3–9]. CO_2 hydrates can be formed at appropriate temperature and pressure in seafloor sediments with water depths greater than 300 m and it is possible to almost completely insulate large amounts of CO_2 through seabed disposal [10–13]. CO_2 is stored in the cages of CO_2 hydrates and the maximum theoretical CO_2 storage capacity of CO_2 hydrates reaches 180.0 V/V [14,15]. The low-permeability artificial CO_2 hydrate layer has been proposed as an effective method to further increase CO_2 storage capacity and prevent CO_2 leakage [16–27], which serves as a stable sealing layer to ensure the safety of oceanic CO_2 sequestration. Therefore, CO_2 sequestration in the form of solid hydrates is a safe and feasible oceanic CO_2 sequestration method.

However, several challenges exist, particularly concerning the risk of CO_2 leakage due to the slow formation of CO_2 hydrates. The studies have found that liquid CO_2 was often encapsulated by a thin hydrate film during hydrate formation [13,28–33], which limited its dissolution and further restricted hydrate growth by reducing the mass transfer of liquid CO_2 [30]. CO_2 hydrate formation kinetics were not enhanced by increasing pressure [34]. Moreover, the presence of salts, such as sodium ions (Na^+), magnesium ions (Mg^{2+}) and chloride ions (Cl^-), in seawater inhibited the gas hydrate formation kinetics by decreasing hydrate growth rate [35–38], and the inhibitory effect of salt ions with high concentrations became more obvious [11,38]. Na^+, Mg^{2+}, Cl^- and sulfate ions (SO_4^{2-}) were solvated via ion–dipole interactions with water molecules, decreasing the activity of water molecules and continuously limiting the available hydrogen bond donor and acceptor sites for hydrate growth [38–41]. CO_2 hydrates in fresh water-saturated systems were more stable than those in brine water-saturated systems, because the amount of salinity affected the stability of CO_2 hydrates [11,41–43]. Low concentrations of salt ions had a negligible impact on CO_2 hydrate stability, while high concentrations of salt ions notably reduced the stability [43]. How to accelerate hydrate formation rate and improve the stability of CO_2 hydrates remains one of the most concerned scientific problems to date.

At present, several thermodynamic and kinetic promoters are employed to promote the rapid CO_2 hydrate formation [44–56]. The tetrahydrofuran (THF) [44,45] and tetrabutylammonium bromide

* Corresponding authors at: School of Chemistry and Chemical Engineering, South China University of Technology, Guangzhou 510640, China (S. Fan).
E-mail addresses: wyh@scut.edu.cn (Y. Wang), ssfan@scut.edu.cn (S. Fan).

https://doi.org/10.1016/j.cej.2025.162749
Received 19 January 2025; Received in revised form 29 March 2025; Accepted 16 April 2025
Available online 16 April 2025

Nomenclature

CO_2	Carbon dioxide
FA	Fulvic acid
K^+	Potassium ion
Na^+	Sodium ion
Mg^{2+}	Magnesium ion
Cl^-	Chloride ion
SO_4^{2-}	Sulfate ion
THF	Tetrahydrofuran
TBAB	Tetrabutylammonium bromide
SDS	Sodium dodecyl sulfate
NaCl	Sodium chloride
Ca^{2+}	Calcium ion
K^+	Potassium ion
Δn_{CO_2}	CO_2 gas consumption
$\Delta n_{CO_2}^H$	Moles of CO_2 captured in hydrate cages
$n_{CO_2}^{gt}$	Moles of CO_2 remaining in the gas phase after the complete dissociation of CO_2 hydrate
n_s^t	Moles of dissolved CO_2 in the solution
$n_{CO_2}^0$	Moles of CO_2 in the gas phase before hydrate dissociation
P	Pressure
T	Temperature
V	Volume of the gas phase
Z	Gas compressibility factor
V_w	Volume of the water
SC	Gas storage capacity of CO_2 hydrate
V_H	Volume of hydrate
M	Hydrate number
v_W^{MT}	Molar volume of the CO_2 hydrate cavity
R_H	Hydrate growth rate
W	Conversion percentage of water to hydrate
Δn_{H_2O}	Conversion moles of water to hydrate
R_W	Conversion rate of water to hydrate
W	Conversion percentage of water to hydrate
ΔV_W^t	Apparent water consumption
d	Diameter of the reactor
R_{WC}	Rate of apparent water consumption
Δn_W	Moles of apparent water consumption
ρ_W	Water density
M_W	Molar mass of water
V_W^0	Water volume at time 0
V_W^t	Water volume at time t
h_0	Initial liquid water height at time 0
h_t	Liquid water height at time t
$\Delta n_{CO_2}^d$	Dissolved amount of liquid CO_2 in the aqueous solution
V_d	Volume of gas storage tank
V_{CO_2}	Volume of liquid CO_2
ρ_{CO_2}	Density of liquid CO_2
M_{CO_2}	Molar mass of liquid CO_2
R_{ve}	Volume expansion rate of water converted into CO_2 hydrate
V_t	Whole volume after hydrate formation
V_0	Whole volume after liquid CO_2 injection
V_c	Volume of liquid CO_2 consumed
C_A	Concentration of additive
C_i	Concentration of salt
t_{in}	Induction time
Rn	Molar ratio of liquid CO_2 to liquid water
Met	L-Methionine
SL	Sodium lignosulfonate

(TBAB) [46,47], as thermodynamic promoters, could moderate phase equilibrium conditions to allow CO_2 hydrate to form at relatively high temperature and low pressure. Sodium dodecyl sulfate (SDS) was proved to help the conversion of water to hydrate with CO_2 and hydrate nucleation was shortened by providing the additional solid–liquid heterogeneous interface in the presence of nanoparticles [56]. Considering the marine ecological environment, these promoters are not viable. Consequently, eco-friendly alternatives, such as amino acids, are investigated. Linga et al. [57,58] demonstrated that L-tryptophan could increase the conversion ratio of water to hydrate to 98.6 % in aqueous solution and 93.8 % in silica sand. The average conversion rates of water to hydrate were 0.0043 mol H_2O/(mol H_2O·min) in aqueous solution and 0.0078 mol H_2O/(mol H_2O·min) in silica sand, which were attributed to the hydrophilic carboxyl and amino groups of L-tryptophan to promote hydrate formation by increasing its local concentration. However, the effect of amino acids was limited in seawater, resulting in a much slow hydrate formation [59]. In the aqueous solution with 3.5 wt % sodium chloride (NaCl), the conversion ratio and the conversion rate of water to hydrate were decreased to 10.0 % and 0.0025 mol H_2O/(mol H_2O·min) respectively [60,61]. Given that seawater reduces the promotion effect of amino acid on CO_2 hydrates formation, finding more efficient and eco-friendly additives has been given high priority to achieve large-scale oceanic CO_2 sequestration.

Organic matters in marine sediments, as green bioactive substances widely existing in nature, can be the potential additives to promote liquid CO_2 to rapidly form CO_2 hydrate, because it has been proven that CO_2 hydrate growth was improved by the extracted suspension from marine sediments of natural gas hydrate layer [62,63]. Furthermore, self-siphoning, an ordinary phenomenon in nature, has been applied in various fields, including coating self-repairing [64], water transport [65], marine oil contamination cleanup [66], life sciences [67] and seawater desalination [68,69]. The self-siphoning achieved self-starting behavior through a pressure difference, transporting water and gas without energy input [68,70], but the “self-siphoning” phenomenon had not been previously observed in the process of gas hydrate formation. In this work, an eco-friendly additive, fulvic acid (FA), was introduced as a promoter of CO_2 hydrate and a “self-siphoning” phenomenon was found to promote CO_2 hydrate formation. FA is produced by biodegradation of dead organic matter, which are the major organic constituents of soil (humus), peat, coal, many upland streams, dystrophic lakes, and ocean water. We investigated the effects of temperature and dosage of FA on hydrate formation from liquid CO_2 in seawater of the South China, and the stability of CO_2 hydrates. Finally, the promotional mechanism of FA on CO_2 hydrate formation was discussed.

2. Experimental

2.1. Materials

FA with a purity of more than 90.0 mol% was purchased from Shanghai Aladdin Biochemical Technology Co. Ltd, China. The seawater of South China Sea was provided by Guangzhou Marine Geological Survey, China. The seawater of South China Sea consists of 0.04 wt% calcium ion (Ca^{2+}), 0.04 wt% potassium ion (K^+), 1.31 wt% Na^+, 0.15 wt% Mg^{2+}, 1.75 wt% Cl^- and 0.26 wt% SO_4^{2-}, as shown in Table 1. CO_2 with a purity of 99.9 mol% was purchased from Guangzhou Shengying Gas Co. Ltd, China.

Table 1
The composition of the components presented in the seawater of South China Sea.

Components	Ca^{2+}	K^+	Na^+	Mg^{2+}	Cl^-	SO_4^{2-}
Concentration /wt%	0.04	0.04	1.31	0.15	1.75	0.26

2.2. Experimental apparatus and procedure

The experimental apparatus included a high-pressure visual reactor, gas cylinder, gas booster pump, water bath, data acquisition system and computer, as shown in Fig. 1. The high-pressure visual reactor was composed of a cylinder with an inner diameter of 30.0 mm and an effective volume of 72.0 mL. Both sides of the reactor were designed with visual windows suitable for observing of the experimental phenomena in the reactor. A thermocouple with an accuracy of ±0.1 K (Shanghai Yijia Electric Heating Co., Ltd.) and a pressure sensor with an accuracy of ±0.01 MPa (Guangzhou Senex Instrument Co., Ltd.) were equipped on the reactor to detect the temperature and pressure. Furthermore, an inverted microscope (Carl Zeiss Axio Observer A1, Germany) was applied to observe the morphology of the aqueous solution of 500 ppm FA before and after CO_2 dissolution. The pH meter and the interfacial tensiometer were employed to measure the pH and interfacial tension of the solution, respectively.

The experiment process of CO_2 hydrate formation by liquid CO_2 was as follows. First, aqueous solutions with different FA concentrations were prepared by mixing the seawater and FA. After 25.0 mL of aqueous solution with FA was added into the reactor, it was cooled by water bath. When the temperature reached the experimental value of 275.2 K, liquid CO_2 was injected into the reactor using gas booster pump. The completion of liquid CO_2 injection was considered as the beginning time of hydrate formation, and CO_2 hydrate morphology during hydrate formation was observed through the visual window. When the liquid water was completely transformed into solid hydrates by the hydrate morphology observation and the temperature and pressure did not change, which indicated that hydrate formation ended. Next, the hydrate dissociation was conducted by decreasing the pressure and heating. The temperature and pressure curves during the hydrate formation and dissociation process were recorded at 10.0 s intervals. The solid hydrates were completely dissociated into the liquid water, and the pressure and temperature no longer increased, showing the completion of hydrate decomposition.

The procedures of Raman test, solubility and pH measurements were as follows. A micro-Raman spectroscopy system (Renishaw Ltd., Gloucester-shire, UK) was used to determine the structure of CO_2 hydrates and identify the occupancy of CO_2 in small cages and large cages. And it was equipped with a 2400 groove/mm grating, a 50 × objective, and a 532 nm laser source. After the synthesis of the hydrates, the hydrates were moved to the liquid nitrogen environment and preserved at low temperature. In the process of testing, the temperature was cooled to 173 K by the Linkam THMSG 600 thermal stage (Linkam Scientific Instruments Ltd, Tadworth, UK). Then, the hydrate samples were quickly placed in the cooling cell on the stage and the micro-Raman spectroscopy was turned on for determination. At last, the structure of CO_2 hydrates and occupancy of CO_2 in small cages and large cages were analyzed by Raman spectroscopy. The solubility of liquid CO_2 was determined using an indirect measurement method. The total moles of CO_2 in the injection system were calculated using an additional connected storage tank. Once CO_2 reached dissolution equilibrium, the remaining amount of CO_2 was calculated. The dissolved amount of liquid CO_2 was calculated as the difference between the total moles of CO_2 initially injected into the system and the remaining CO_2. During hydrate formation, the remaining aqueous solution was collected in a beaker, and the pH of the aqueous solution was determined using a pH meter with an accuracy of ±0.02 pH.

2.3. Data processing

CO_2 gas consumption at time t (Δn_{CO_2}) in the solution with additive concentration is defined as the difference between the moles of CO_2 injected into the reactor at the beginning and the moles of CO_2 remaining in the reactor at the end of hydrate formation. However, since the consumption of liquid CO_2 is not easy to measure, the moles of CO_2 captured in hydrate cages ($\Delta n^H_{CO_2}$) can be obtained by hydrate dissociation to release CO_2 in this work, as shown in Equation (1).

$$\Delta n^H_{CO_2} = n^t_{CO_2} - n^0_{CO_2} = n^{gt}_{CO_2} + n^t_s - n^0_{CO_2} \quad (1)$$

where $n^t_{CO_2}$ is the sum of the moles of CO_2 remaining in the gas phase after the complete dissociation of CO_2 hydrates ($n^{gt}_{CO_2}$) and the moles of dissolved CO_2 in the solution (n^t_s), $n^0_{CO_2}$ is the moles of CO_2 in the gas

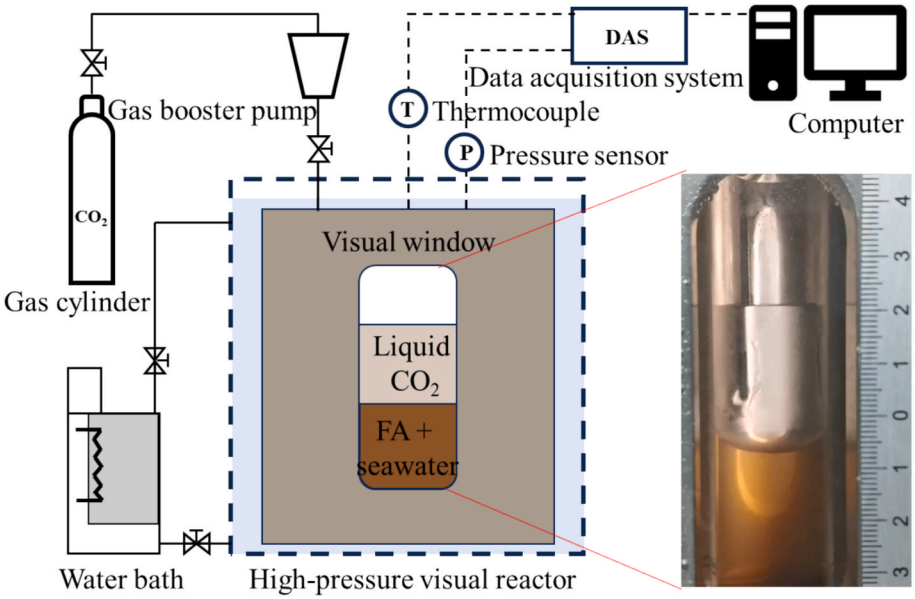

Fig. 1. Experimental apparatus of CO_2 hydrate formation from liquid CO_2.

phase before hydrate dissociation.

The moles of CO_2 remaining in the gas phase after the complete dissociation of CO_2 hydrates ($n^{gt}_{CO_2}$) is calculated by Equation (2).

$$n^{gt}_{CO_2} = \frac{P_t V_t}{Z_t R T_t} \tag{2}$$

where P_t, T_t and V_t are the pressure, temperature and volume of the gas phase after the complete dissociation of CO_2 hydrates respectively, R is the ideal gas constant, Z_t is the gas compressibility factor obtained from Peng-Robinson Equation.

The moles of dissolved CO_2 in the solution (n^t_s) at the end of the hydrate dissociation is calculated by Equation (3) [71].

$$n^t_s = P_t/(13.99194 - 2650.11724/(T_t + 273.15)) \times 0.999846 \times V_w/18 \tag{3}$$

where V_w represents the volume of the water in the reactor at the end of the hydrate dissociation.

The moles of CO_2 in the gas phase before the complete dissociation of CO_2 hydrates ($n^0_{CO_2}$) is calculated by Equation (4).

$$n^0_{CO_2} = \frac{P_0 V_0}{Z_0 R T_0} \tag{4}$$

where P_0, T_0 and V_0 are the pressure, temperature and volume of the gas phase before the hydrate dissociation respectively, Z_0 is the gas compressibility factor.

The gas storage capacity of CO_2 hydrates (SC) is defined as the volume of gas released per volume of hydrate at 273.15 K and 101.3 kPa, which is calculated by Equation (5):

$$SC = \frac{V_{STP}}{V_H} = \frac{\frac{\Delta n^H_{CO_2} R T_{STP}}{P_{STP}}}{V_H} \tag{5}$$

where T_{STP} and P_{STP} are respectively the temperature and pressure of the gas phase under standard conditions (273.15 K, 101.3 kPa), R is the ideal gas constant, V_H is the volume of hydrates.

The volume of hydrate can be calculated by Equation (6) [72].

$$V_{Ht} = M \times \Delta n_{CO_2} \times v^{MT}_W \tag{6}$$

Where M is the hydrate number and its value is 7.03 [58], v^{MT}_W is the molar volume of the CO_2 hydrate cavity.

The molar volume of the CO_2 hydrate cavity can be calculated by Equation (7) [73].

$$v^{MT}_W = \left[\left(11.835 + 2.217 \times 10^{-5} T + 2.242 \times 10^{-6} T^2\right)^3 \times \frac{10^{-30} N_A}{46} - 8.006 \times 10^{-9} P + 5.448 \times 10^{-12} P^2\right] \times 10^6 \tag{7}$$

Where P is the pressure in the reactor, T is the temperature in the reactor, N_A is Avogadro's constant.

The hydrate growth rate (R_H) can be used to describe the rapidity of hydrate formation, as shown in Equation (8):

$$R_H = \frac{\Delta n^H_{CO_2}}{n^0_{H_2O} \Delta t} \tag{8}$$

where $\Delta n^H_{CO_2}$ is the moles of CO_2 captured in hydrate cages, $n^0_{H_2O}$ is the moles of water added at the beginning of the experiment, Δt is the time between the beginning of hydrate growth and the complete end of hydrate growth.

Conversion percentage of water to hydrate (W) is calculated by Equation (9):

$$W = \frac{\Delta n_{H_2O}}{n^0_{H_2O}} \tag{9}$$

where Δn_{H_2O} is the conversion moles of water to hydrate, $n^0_{H_2O}$ is the moles of water injected into the reactor at the beginning.

Conversion rate of water to hydrate (R_W) is used to describe how quickly water is converted into hydrate, as shown in Equation (10):

$$R_W = \frac{W}{\Delta t} \tag{10}$$

where W is the conversion percentage of water to hydrate, Δt is the time between the beginning of hydrate growth and the complete end of hydrate growth.

Apparent water consumption (ΔV^t_W) is calculated by Equation (11):

$$\Delta V^t_W = V^0_W - V^t_W = \Pi d(h_0 - h_t) \tag{11}$$

where V^0_W is the water volume at time 0, V^t_W is the water volume at time t, d is the diameter of the reactor, h_0 is the initial liquid water height at time 0, h_t is the liquid water height at time t.

Rate of apparent water consumption (R_{WC}) is calculated by Equation (12):

$$R_{WC} = \frac{\Delta n_W}{\Delta t} = \frac{\frac{\Delta V^t_W \rho_W}{M_W}}{\Delta t} \tag{12}$$

where Δn_W is the moles of apparent water consumption, ρ_W is water density, M_W is the molar mass of water, Δt is the time after the beginning of apparent water consumption.

The dissolved amount of liquid CO_2 in the aqueous solution ($\Delta n^d_{CO_2}$) is calculated as the difference between the total moles of CO_2 initially injected into the system ($n^{d0}_{CO_2}$) and the remaining CO_2 ($n^{de}_{CO_2}$), as shown in Equation (13):

$$\Delta n^d_{CO_2} = n^{d0}_{CO_2} - n^{de}_{CO_2} = \frac{P_{d0} V_d}{Z_{d0} R T_{d0}} - \frac{P_{de} V_d}{Z_{de} R T_{de}} - \frac{V_{CO_2} \rho_{CO_2}}{M_{CO_2}} \tag{13}$$

where P_{d0} and T_{d0} are the pressure and temperature in the gas storage tank respectively, P_{de} and T_{de} are the pressure and temperature at CO_2 dissolution equilibrium in the gas storage tank respectively, Z_{d0} and Z_{de} are the gas compressibility factors obtained from Peng-Robinson Equation, V_d is the volume of gas storage tank, V_{CO_2} is the volume of liquid CO_2, ρ_{CO_2} is the density of liquid CO_2, M_{CO_2} is the molar mass of liquid CO_2.

The volume expansion rate of water converted into CO_2 hydrate (R_{ve}) is calculated by Equation (14):

$$R_{ve} = (V_t - V_0 + V_c)/V_0 \tag{14}$$

where V_t is the whole volume after hydrate formation, V_0 is the whole volume after liquid CO_2 injection, V_c is the volume of liquid CO_2 consumed.

3. Results and discussion

3.1. Morphology evolution of rapid hydrate formation with FA from liquid CO_2

The hydrate morphology can provide direct insight into the rapid hydrate nucleation and growth processes from liquid CO_2. Compared to the seawater of South China Sea, the addition of FA effectively overcame the mass transfer limitations imposed by CO_2 hydrate film at the interface between liquid CO_2 and the aqueous solution, thereby facilitating the accelerated growth of the film, as illustrated in Fig. 2. In the seawater of South China Sea without FA, a thin film of CO_2 hydrate at the interface was formed at 18.0 min, but it did not grow further within 240.0 min, as depicted in Fig. 2a and Video SV1 of the supplementary information. The induction time of CO_2 hydrate nucleation and the hydrate growth time were reduced significantly by the low dosage of FA. The

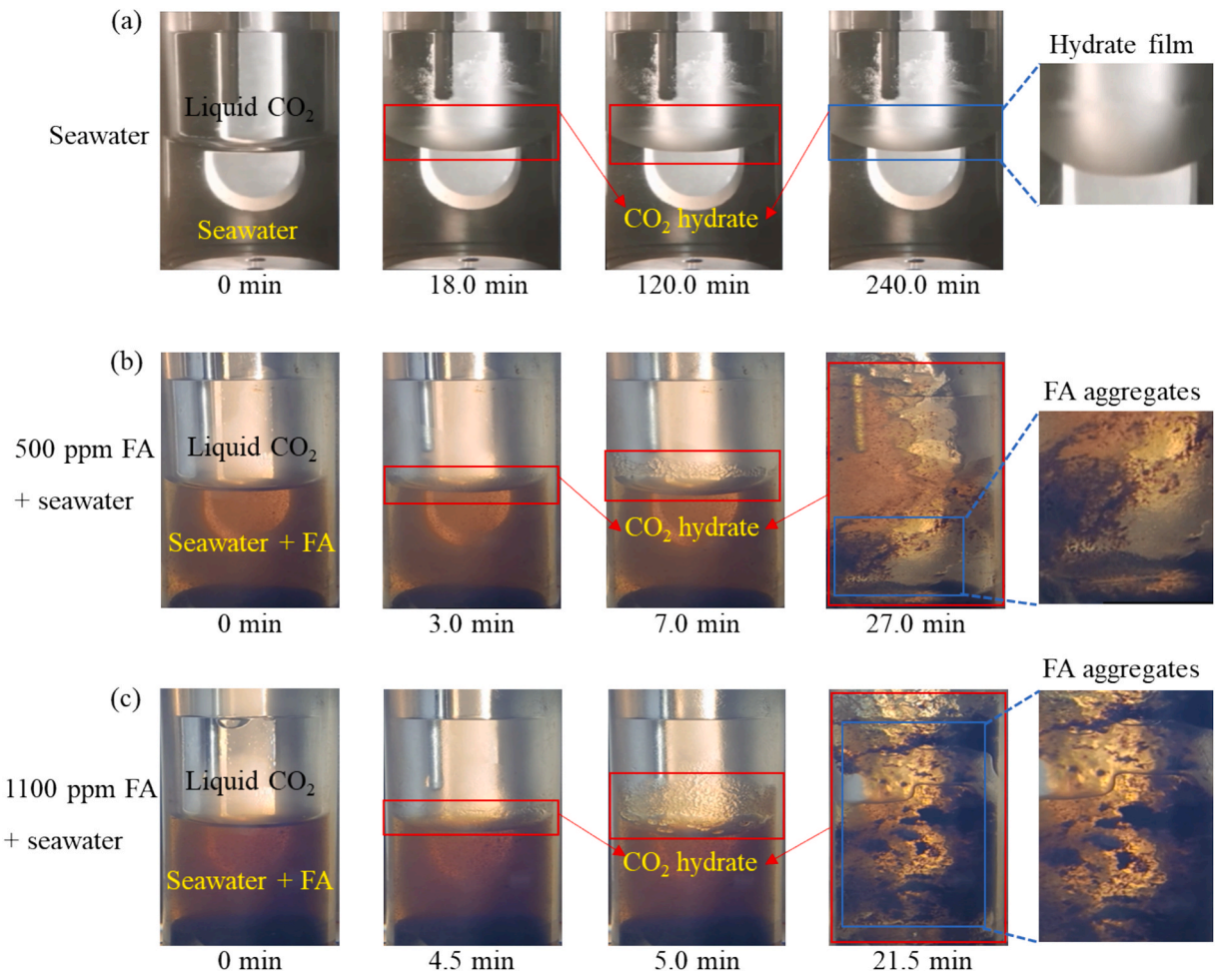

Fig. 2. Morphology evolution of CO_2 hydrate formation from liquid CO_2 in the seawater of South China Sea with (a) without FA, (b) with 500 ppm FA and (c) with 1100 ppm FA at 4.0 MPa and 275.2 K.

induction time of CO_2 hydrate nucleation was determined by the observing the first occurrence of the hydrate film at the interface. Upon injecting liquid CO_2, CO_2 hydrate nucleation and growth were completed within 30.0 min, as shown in Video SV2, Video SV3 and Video SV4 of the supplementary information. In aqueous solutions with 500 ppm and 1100 ppm FA, a hydrate film formed at the liquid CO_2 and water interface within 3.0 min and 4.5 min respectively, and then the hydrate film subsequently grew rapidly, initiating at 7.0 min and 5.0 min, with solid hydrate formation increasing as liquid water was gradually consumed, as illustrated in Fig. 2b and 2c. CO_2 hydrate growth expanded both upward into the liquid CO_2 phase by climbing wall of reactor and downward into the aqueous phase, with a portion of the aqueous solution absorbed into hydrate pores to promote rapid CO_2 hydrate growth. Even as CO_2 was consumed, the height of solid hydrate layer exceeded the initial liquid CO_2 level in the reactor. In the early stage of hydrate growth, the significant liquid tunnels through the dense hydrate layer were constructed to induce FA aggregates (containing FA and water molecules) to enter the space among solid hydrates, resulting in full contact between liquid CO_2 and the aqueous solution.

During this rapid hydrate growth, the temperature in the reactor increased due to heat released from the recombination of hydrogen bonds among water molecules, as illustrated in Fig. S1 of the supplementary information. The aqueous solution was almost fully converted to solid hydrate within 27.0 min and 21.5 min respectively in the aqueous solutions with 500 ppm and 1100 ppm FA, as presented in Fig. 2b and 2c. In the later stage of hydrate growth, "self-siphoning" phenomenon was observed, where FA aggregates migrated to the upper hydrate pores, thus providing more water molecules for CO_2 hydrate growth. Fig. S2 of the supplementary information shows the morphology of CO_2 hydrate formation at other FA concentrations. During the formation of CO_2 hydrate, the volume expansion rate of water converted into CO_2 hydrates was 1.17–1.25, indicating the hydrates constructed with FA were porous and FA played a key role in bridging the hydrates. And the gaps among flaky-like hydrates or scale-like hydrates formed channels for the mass transfer of the aqueous solution, as presented in Fig. S3 of the supplementary information. Therefore, the unique morphology of the FA-containing hydrates was responsible for the occurrence of the novel phenomenon, which subsequently promoted hydrate growth.

At the same concentration, FA maintained a strong promoting effect even as the temperature increased, as reflected in the evolution of hydrate morphology. When the temperature reached 277.2 K and 279.2 K, the conversion from liquid CO_2 to solid hydrates was completed within 24.0 min and 28.0 min in the aqueous solution of 500 ppm FA, respectively, with nearly all liquid water consumed, as shown in Fig. 3. Specifically, at the temperatures of 277.2 K and 279.2 K, a thin hydrate film formed at the interface between liquid CO_2 and the aqueous solution, initiating rapid hydrate growth at 5.0 min and 6.0 min, respectively, and progressing to the bottom of the reactor within 21.0 min and 23.0 min, respectively. However, the increase in temperature resulted in significant differences in the morphology of CO_2 hydrates. CO_2 hydrates displayed dense scale-like, flaky-like, and granular-like structures at 275.2 K, 277.2 K and 279.2 K, respectively. When the temperature increased to 280.2 K, the remaining liquid water in the solution phase

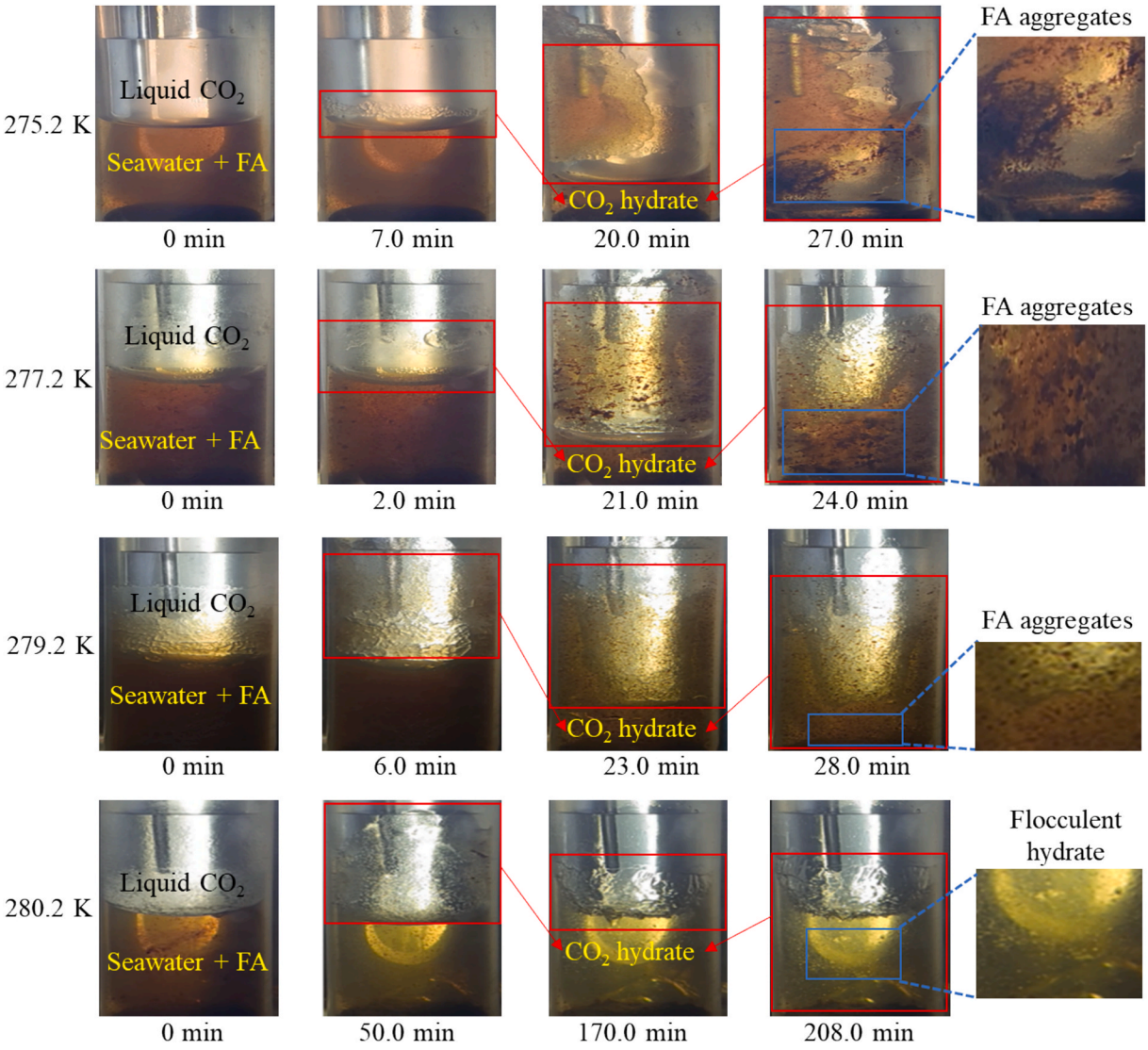

Fig. 3. Morphology evolution of CO_2 hydrate formation from liquid CO_2 in the seawater of South China Sea with 500 ppm FA at 4.0 MPa, 275.2 K, 277.2 K, 279.2 K and 280.2 K.

transformed into flocculent hydrates, and a part of hydrates decomposed and then further grew after 50.0 min. As the driving force of temperature decreased, it not only induced a transformation in the morphology of the CO_2 hydrates but also weakened the "self-siphoning" phenomenon, which was reflected in the progressively smaller area over which the FA aggregates migrated into the hydrate region.

3.2. Kinetic evaluation of rapid hydrate formation with FA from liquid CO_2

After discussing the morphology of the hydrates, the kinetics of the rapid CO_2 hydrate formation process were further investigated and compared. A summary of experimental parameters in the seawater of South China Sea with different FA concentrations was provided in Table 2. The gas storage capacity of CO_2 hydrates and average hydrate growth rate were presented in Fig. 4. The gas storage capacities of CO_2 hydrate were 107.0 V/V, 121.8 V/V, 103.0 V/V, 97.1 V/V and 54.7 V/V for 100 ppm, 500 ppm, 800 ppm, 1100 ppm and 1500 ppm concentrations, respectively, as observed in Fig. 4a. The gas storage capacity of CO_2 hydrate with 500 ppm FA was the largest, with an increase of 26.0 % and 25.4 % compared to 300 ppm and 1100 ppm, respectively. When the FA concentration reached 1500 ppm, it was also significantly reduced, and the hydrate growth was notably inhibited. The average CO_2 hydrate growth rate also presented a similar trend to the gas storage capacity of CO_2 hydrates. With the increase of FA concentration, it firstly increased and then decreased, as revealed in Fig. 4b. The average hydrate growth rate at FA concentrations ranging from 300 ppm to 1100 ppm was significantly higher than that of 100 ppm and 1500 ppm. In the aqueous solution of 500 ppm FA, it reached the maximum value of 4.11 mmol CO_2/(mol H_2O·min), but it was close to 3.37 mmol CO_2/(mol H_2O•min) and 3.96 mmol CO_2/(mol H_2O·min) in aqueous solutions of 800 ppm and 1100 ppm FA. The results demonstrated that the presence of FA significantly enhanced the formation rate of CO_2 hydrates from liquid CO_2 in the seawater of the South China Sea.

In addition to liquid CO_2 consumption, water utilization efficiency is also critical, as shown in Fig. 5. In the first 30.0 min, the apparent water consumption increased linearly for FA concentrations ranging from 300 ppm to 1100 ppm and was significantly higher than that for 100 ppm and 1500 ppm FA, until 25.0 mL of water was completely consumed, as described in Fig. 5a. For 1500 ppm FA, only 10.2 mL was consumed after 40.0 min. Fig. S4 of the supplementary information shows the conversion percentage of water to hydrate and rate of apparent water consumption. The conversion percentage of water to hydrate with 90.2 % was the largest. The average conversion rate of water to hydrate was

Table 2
A summary of experimental parameters in the seawater of South China Sea with additives at 275.2 K and 4.0 MPa.

System	C_A /ppm	t_{in}/min	Δt /min	R_H /(mmol CO_2/(mol H_2O·min))	SC/(V/V)	R_W /(mol H_2O/(mol H_2O·min))	W/%
Seawater + Rn = 1:3 + 275.2 K	0	18	0	0	0	0	0
Seawater + FA +	100	6.0	123.0	0.70	107.0	0.006	79.2
Rn = 1:3 + 275.2 K	100	5.0	102.0	0.84	107.1	0.008	79.3
	300	5.0	30.0	2.62	97.9	0.024	72.5
	300	4.0	32.0	2.24	89.1	0.021	66.0
	300	7.0	26.0	3.18	102.9	0.029	76.3
	500	4.5	27.0	3.80	127.8	0.035	94.7
	500	3	20.0	4.46	111.0	0.041	82.2
	500	2	25.0	4.07	126.6	0.038	93.8
	800	4.5	25.0	3.60	111.9	0.033	82.9
	800	4.0	26.0	3.00	97.2	0.028	72.0
	800	8.0	23.0	3.50	100.1	0.032	74.1
	1100	7.5	22.0	3.92	107.4	0.036	79.6
	1100	5.0	21.0	3.73	97.5	0.034	72.2
	1100	4.0	16.5	4.21	86.5	0.039	64.1
	1500	3.5	47.0	0.93	54.2	0.009	40.2
	1500	10.5	50.0	0.89	55.1	0.008	40.8
Seawater + FA +	500	4.0	26.0	2.79	90.2	0.026	66.8
Rn = 1:6 + 275.2 K	500	1.0	25.0	2.14	66.5	0.020	49.3
Seawater + FA +	500	3.0	28.0	2.06	71.8	0.019	53.2
Rn = 1:12 + 275.2 K	500	2.0	29.0	1.97	71.1	0.018	52.7
Seawater + FA +	500	0	22	2.47	89.2	0.030	66.0
Rn = 1:3 + 277.2 K	500	0.5	25	2.29	82.5	0.024	61.1
Seawater + FA +	500	0	28	2.43	87.9	0.024	65.1
Rn = 1:3 + 279.2 K	500	0	29	1.90	68.5	0.018	50.8

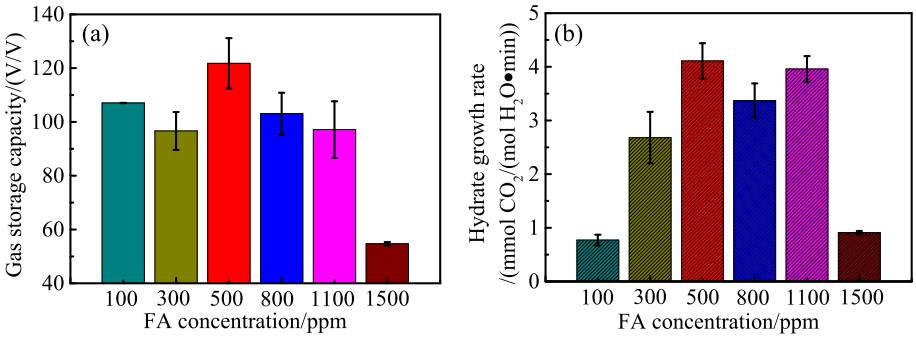

Fig. 4. (a) Gas storage capacity of CO_2 hydrates and (b) Average hydrate growth rate in the seawater of South China Sea with different FA concentrations at 4.0 MPa and 275.2 K.

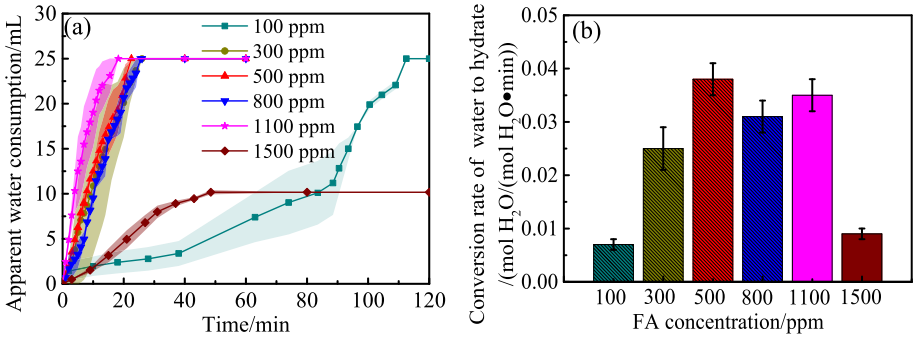

Fig. 5. (a) Apparent water consumption for hydrate formation process and (b) Average conversion rate of water to hydrate in the seawater of South China Sea with different FA concentrations at 4.0 MPa and 275.2 K.

higher than 0.031 mol H_2O/(mol H_2O·min) in aqueous solutions with FA concentrations ranging from 500 ppm to 1100 ppm, but it was significantly reduced to 0.007 mol H_2O/(mol H_2O·min) for 100 ppm, as seen in Fig. 5b. The maximum conversion rate of 0.038 mol H_2O/(mol H_2O·min) was achieved in the aqueous solution with 500 ppm FA.

Fig. 6 represents the Raman spectra of CO_2 hydrates formed in the seawater of South China Sea with 500 ppm FA. The peaks at 1275.8 cm^{-1} and 1380.3 cm^{-1} corresponded to the stretching vibration of large cages ($5^{12}6^2$) for sI CO_2 hydrates in the seawater of South China Sea without FA, which were similar with the experimental results of Gborigi et al [74,75]. And the peaks at 1276.0 cm^{-1} and 1379.4 cm^{-1} belonged to the stretching vibration of large cages for sI CO_2 hydrate in the

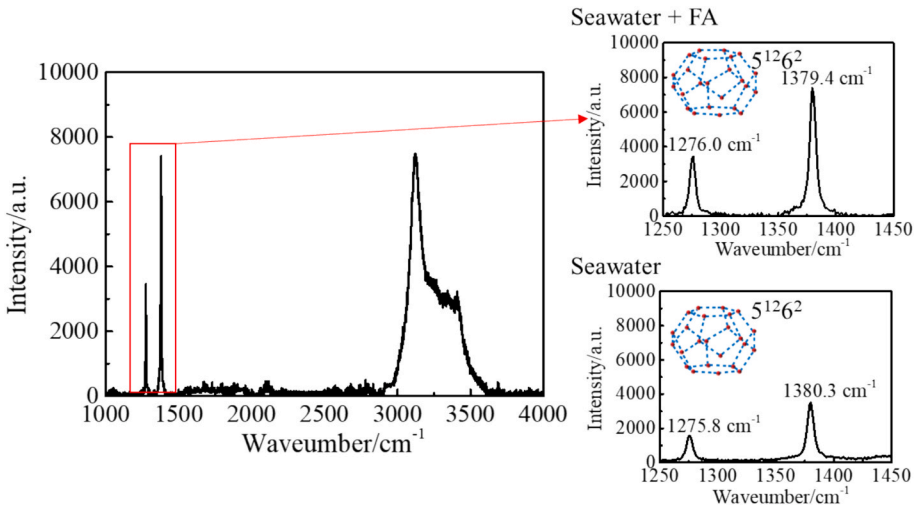

Fig. 6. Raman spectra of CO_2 hydrate formed in the seawater of South China Sea with 500 ppm FA.

seawater of South China Sea with 500 ppm FA. It could be seen that CO_2 molecules mainly occupied the large cages of sI CO_2 hydrate, with difficulty in entering the small cages, resulting in a gas storage capacity close to the theoretical value of 135.0 V/V. In the hydrate structure, only the CO_2 peak and the ice peak were observed, with no FA peak detected, indicating that FA molecules were not incorporated into the hydrate cages.

After confirming the optimal FA concentration, the effects of liquid CO_2 content and temperature variations on FA's ability to promote hydrate formation were systematically investigated, as presented in Fig. 7. In theory, when the hydrate cages are completely occupied by CO_2 molecules, the molar ratio of CO_2 molecules to water molecules is 1:5.75. When the molar ratio of liquid CO_2 to liquid water (Rn) was decreased to 1:6 and 1:12, the gas storage capacities of CO_2 hydrates decreased to 78.4 V/V and 71.4 V/V, respectively, and the average hydrate growth rates were 2.46 mmol CO_2/(mol H_2O·min) and 2.02 mmol CO_2/(mol H_2O·min), respectively, as presented in Fig. 7a. Insufficient liquid CO_2 resulted in the formation of flocculent hydrates, thereby reducing the gas storage capacity of the hydrates. At the molar ratio of liquid CO_2 to liquid water of 1:3, when the temperature increased to 277.2 K and 279.2 K, the gas storage capacities of CO_2 hydrates decreased to 85.8 V/V and 78.2 V/V, respectively, with corresponding the average hydrate growth rates were 2.34 mmol CO_2/(mol H_2O·min) and 2.17 mmol CO_2/(mol H_2O·min), respectively, as illustrated in Fig. 7b. Although the hydrate growth time was significantly shortened at high temperature, the reduced gas storage capacity observed in Fig. 7b caused a slight decrease in the hydrate growth rate. Nevertheless, even high temperature and low dosage of liquid CO_2, the hydrate growth rate consistently exceeded 2.00 mmol CO_2/(mol H_2O·min), highlighting the sustained ability of FA to effectively promote hydrate formation.

According to the above results, 500 ppm FA, a molar ratio of liquid CO_2 and liquid water of 1:3 and 275.2 K were the optimal conditions. Therefore, CO_2 hydrate formation with 500 ppm SDS was compared under the same condition, and no obvious growth of hydrate crystals was observed within 240.0 min, as presented in Fig. S5 of the supplementary information. Table 3 summarizes that the conversion percentage of water to hydrate and average conversion rate of water to hydrate in different CO_2 hydrate formation conditions. The conversion percentage of water to hydrate and average conversion rate of water to hydrate with 500 ppm FA were 2.1 and 5.4 times higher than those of optimal 1500 ppm SDS, respectively. In recent years, various additives have been used to enhance CO_2 hydrate formation, and the hydrate formation process has been analyzed using these parameters. The conversion percentage of water to hydrate and conversion rate of water to hydrate in the presence of amino acids for liquid CO_2 were higher than that for gas CO_2 [57,58,76–78], which was attributed to an excess amount of CO_2 to overcome the mass transfer barrier. 1,3-dioxolane could significantly promote methane hydrate formation [79,80], but its ability to promote CO_2 hydrate was limited. The conversion rate of water to hydrate in the FA system in our work was higher than that in other systems. Even under static conditions, the average conversion rate of water to hydrate with FA was 8.8 times higher than that of amino acids under agitation system [57], and 237.5 times higher than that of amino acids under static system [59]. Compared with threonine and sodium lignosulfonate (SL), it was also increased significantly [81,82]. FA has a more efficient ability to act as a promoter under liquid CO_2, accelerating the hydrate formation by 1–2 orders of magnitude.

3.3. CO_2 hydrate dissociation with FA by temperature increase

To demonstrate that FA plays a key role in stabilizing the hydrate

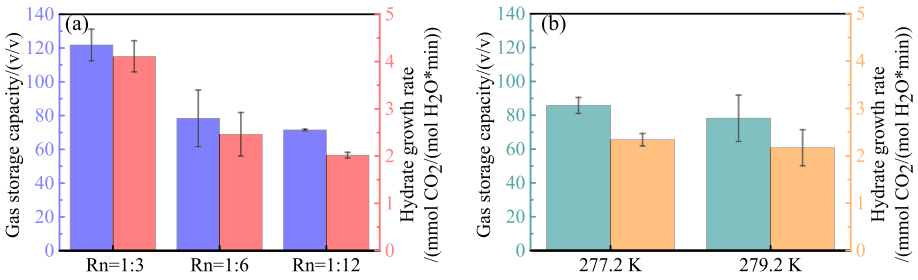

Fig. 7. Gas storage capacity of CO_2 hydrates and average hydrate growth rate in the seawater of South China Sea containing 500 ppm FA with (a) Different molar ratios of liquid CO_2 and liquid water at 4.0 MPa and 275.2 K and (b) Different temperatures at Rn = 1:3.

Table 3
A summary of conversion percentage of water to hydrate (W) and average conversion rate of water to hydrate (R_W) in different CO_2 hydrate formation conditions.

CO_2 phase	Additive	C_A	C_i	T/K	P/MPa	W/%	Average R_W/(mol H_2O/(mol H_2O·min))	Reference
Gas CO_2	SDS	500 ppm	0 wt%	273.6	3.0	42.8	0.021	[48]
	Met	0.2 wt%	0 wt%	275.2	2.8	17.9	0.00067	[76]
	THF + Met	1.0 mol %	0 wt%	275.2	3.4	4.1	0.00046	[77]
Liquid CO_2	NaCl	3.5 wt%	3.5 wt%	277.2	6.0	10.0	0.0025	[60]
	SDS	288 ppm	0 wt%	274.0	6.0	1.4	0.00055	[61]
	SDS	0.05 wt%	0 wt%	274.2	4.0	70.6	0.0059	[56]
	SDS + SiO_2	0.05 wt%		274.2	4.0	64.9	0.0054	
	L-tryptophan	0 ppm	0 wt%	274.2	6.4	58.0	0.00081	[57]
		500 ppm		274.2	6.4	98.8	0.0035	
		1000 ppm		274.2	6.4	98.6	0.0043	
	SL	1.0 wt%	0 wt%	288.0	6.0	31.8	0.00039	[81]
		3.0 wt%		288.0	6.0	28.5	0.00035	
	L-tryptophan	0 ppm	3.5 wt%	274.6	10.0	25.0	0.00017	[59]
		500 ppm		274.6	10.0	19.2	0.00016	
	Threonine	1×10^{-5} mol %	3.55 wt%	275.2	4.0	68.4	0.0044	[82]
	SDS	1500 ppm	3.55 wt%	275.2	4.0	43.7	0.0070	This work
	FA	500 ppm		275.2	4.0	90.2	0.038	This work

structure, the dissociation characteristics of CO_2 hydrates containing FA were investigated by increasing the temperature. Before CO_2 hydrate dissociation, the residual liquid CO_2 in the gap between solid CO_2 hydrates was released, and the pressure decreased from 4.0 MPa to 3.0 MPa, as described in Fig. S1 of the supplementary information. Then, the pressure of 3.0 MPa plateaued for a period during pressure release and prior temperature rise, which indicated the stability of the overall hydrate skeleton remained unaffected by the 1.0 MPa pressure decrease and the 9.0 K temperature increase. When the dissociation temperature reached 284.2 K, solid CO_2 hydrates began to decompose, as revealed in Fig. 8. The hydrates near the reactor wall decomposed first to FA aqueous solution (Video SV5 of the supplementary information). At 20.0 min, part of the aqueous solution has occurred, and the columnar shape of the hydrates maintained in the early stage of hydrate decomposition, as presented in Fig. 8a. FA was located within the gaps of the hydrate crystals, effectively stabilizing the framework structure of the hydrates. The solid hydrates were basically immersed in the aqueous solution at 60.0 min, and there were no obvious solid hydrates in the aqueous solution at 103.0 min. Fig. S6 of the supplementary information shows the morphology of CO_2 hydrates in the process of hydrate dissociation with different FA concentrations. The Raman spectra revealed that the crystal structure of CO_2 hydrates remained stable for the first 15.0 min, with no CO_2 molecules escaping from the hydrate cages, as depicted in Fig. 8b. After the peak of the hydrate cages (3131 cm^{-1}) disappeared, CO_2 molecules were also released from large cages. Because the solid hydrates formed were denser, the dissociation time extended. FA makes CO_2 hydrates more compact and stable by bridging the hydrate structures, which is advantageous for the safety of oceanic

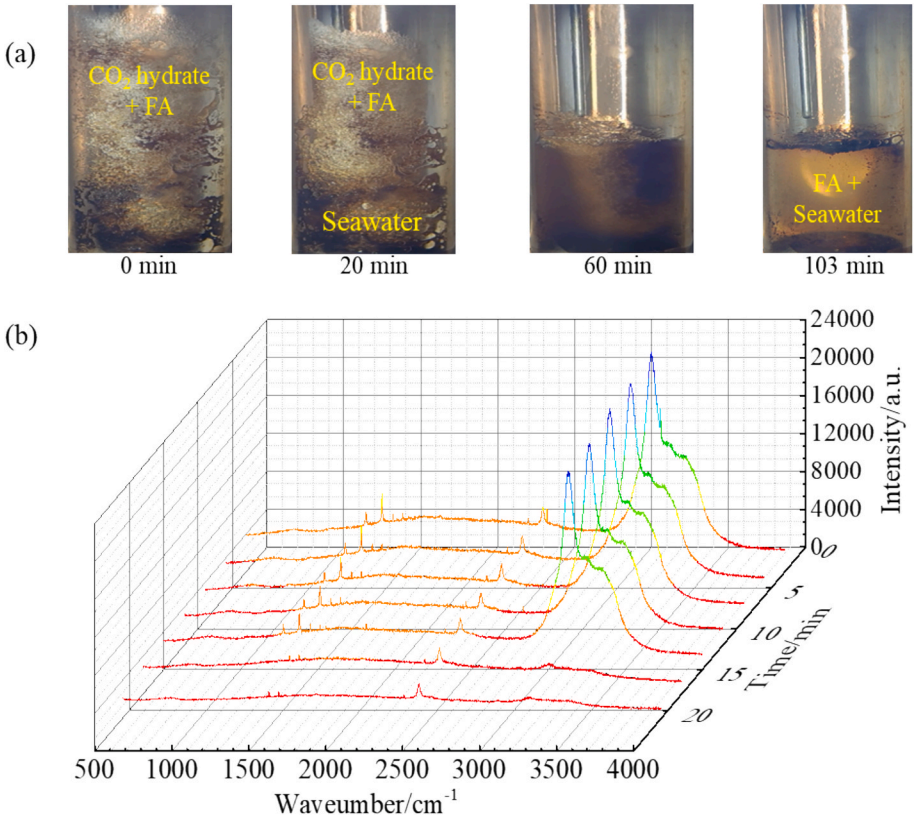

Fig. 8. (a) Morphology evolution and (b) Raman spectra of CO_2 hydrates in the process of hydrate dissociation for 500 ppm FA.

CO_2 sequestration.

3.4. CO_2 hydrate growth mechanism via self-siphoning principle

The "self-siphoning" of water clusters was significantly observed after hydrate formation, as shown in the Fig. 9. The blue line is the migration direction. Before hydrate formation, water microclusters containing FA gradually moved towards the liquid–liquid interface upon the injection of liquid CO_2. After hydrate formation, the phenomenon of "self-siphoning" occurred and the aqueous solution was spontaneously sucked into the hydrate pores more quickly, exhibiting a consistent behavior akin to self-siphoning in U-shaped tubes. Therefore, this phenomenon was considered as the "self-siphoning" phenomenon. Once liquid water was consumed, FA aggregations also entered the hydrate layers at the top of the reactor. As the FA concentration increased, "self-siphoning" of water clusters became more pronounced. The migration heights of water clusters were 27 mm, 32 mm and 51 mm in the aqueous solution of 500 ppm, 800 ppm and 1100 ppm FA respectively, as presented in Fig. 9a, Fig. 9b and Fig. 9c. The more obvious "self-siphoning" phenomenon occurred in the late stage of hydrate growth, as presented in the Video SV1, Video SV2 and Video SV3 of the supplementary information. This phenomenon was clearly observed in more local areas in the aqueous solution with 1100 ppm FA, as shown in Fig. 10. The water clusters containing FA and H_2O molecules water were introduced into the CO_2 hydrate pores along the mass transfer channel between hydrates. The experiment showed that the aqueous solution containing FA, in the absence of solid hydrates, also migrated into the liquid CO_2 phase along the wall of the reactor, as described in Fig. S7 of the

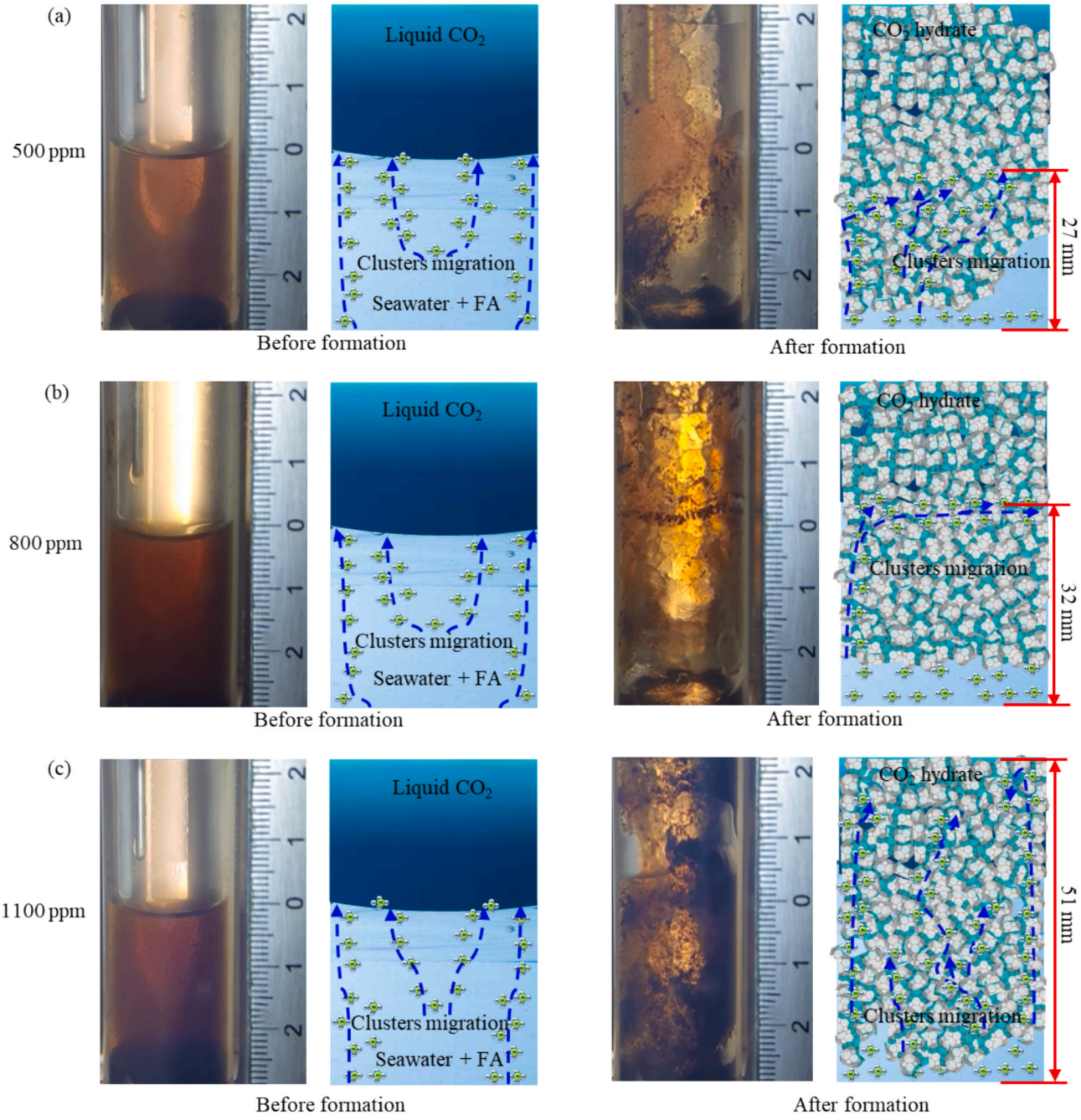

Fig. 9. "Self-siphoning" of water clusters after hydrate formation in the seawater of South China Sea with (a) 500 ppm FA, (b) 800 ppm FA and (c) 1100 ppm FA at 4.0 MPa and 275.2 K. The blue line is the migration direction.

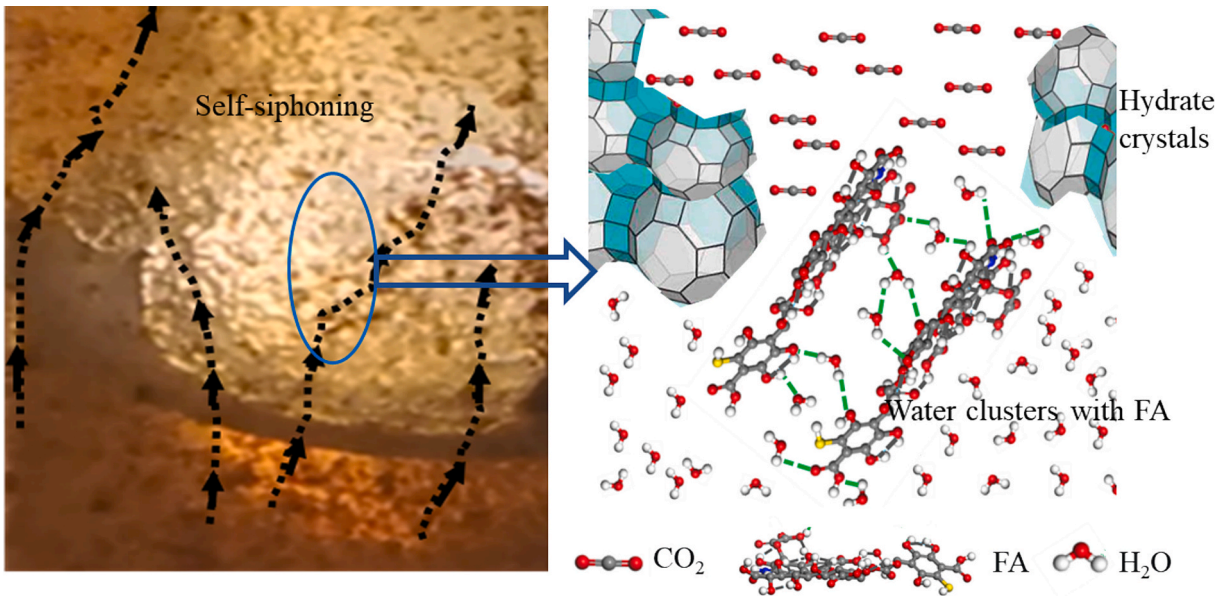

Fig. 10. "Self-siphoning" of water clusters during the hydrate formation from liquid CO_2 in the seawater of South China Sea with FA.

supplementary information.

The reason for the formation of "self-siphoning" phenomenon was demonstrated through a series of experiments. First, to determine whether FA affects the thermodynamics of CO_2 hydrates, the phase equilibria of CO_2 hydrates in the aqueous solution with 500 ppm FA was determined through the isochoric pressure search method. The experimental results showed that the phase equilibria pressure and temperature of pure water system were consistent with that in our previous results [83], and FA did not change the phase equilibria pressure and temperature of CO_2 hydrate formation in the seawater, as presented in Fig. 11. The nanoparticles were used as labeled materials to investigate the effect of temperature difference in the process of CO_2 injection on the "self-siphoning" phenomenon. And the results showed that the temperature increase of the aqueous solution caused irregular thermal motion rather than the "self-siphoning" phenomenon, as illustrated in Fig. S8 and Fig. S9 of the supplementary information. In the first 3.0 min of liquid CO_2 injection, the nanoparticles rapidly expanded the whole solution, but they slowly settled to the bottom of the reactor after 7.0 min, as shown in Fig. S9 of the supplementary information. When the temperature of liquid CO_2 was cooled to 275.2 K in the aqueous solution

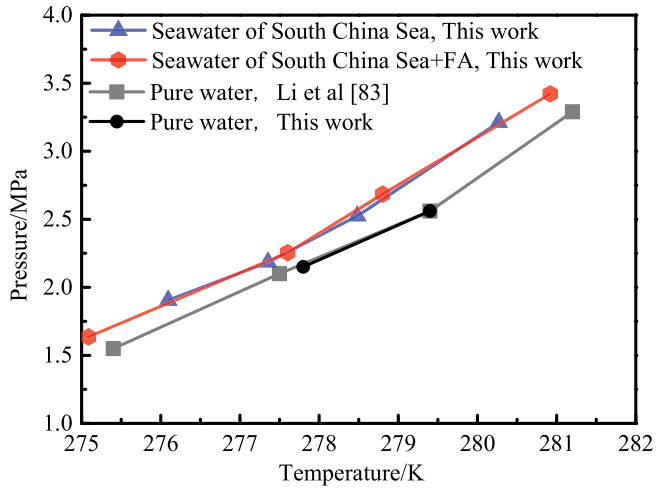

Fig. 11. Experimental phase equilibria of CO_2 hydrate in pure water, seawater of South China Sea and seawater of South China Sea with 500 ppm FA.

with FA, "self-siphoning" was also observed without a temperature difference, as described in Fig. 12. Many water clusters moved regularly towards the liquid–liquid interface before the hydrate growth, and then they were sucked into the hydrate pores to replenish water for hydrate growth, as presented in Fig. 12a. The temperature of the solution phase did not increase significantly in the process of liquid CO_2 injection and hydrate growth within 30.0 min, as shown in Fig. 12b. CO_2 hydrate formation with labeled nanoparticle materials, and without a temperature difference, confirmed that "self-siphoning" was not thermo-siphoning due to temperature difference.

The "self-siphoning" phenomenon became more pronounced after CO_2 dissolution, as revealed in Fig. S10 of the supplementary information. The 40x microscope showed that many clusters owned directional migration after CO_2 was dissolved in FA aqueous solution, but no distinct water clusters were evident before CO_2 dissolution, as depicted in Fig. S11 and Fig. S12 of the supplementary information. Subsequently, the interactions between CO_2 and water enhanced by FA were systematically studied through CO_2 solubility, pH value and interface tension measurements, as shown in the Fig. 13. The CO_2 solubility significantly increased in the presence of FA, with the dissolved amounts of gas and liquid CO_2 at equilibrium in FA-containing seawater reaching 0.057 mol and 0.059 mol, respectively, both exceeding the corresponding dissolved amount in seawater, as illustrated in Fig. 13a. Moreover, the dissolution rate of CO_2, both in gaseous and liquid forms, was notably higher in FA-containing seawater compared to that in seawater. For liquid CO_2, CO_2 solubility in aqueous solution of 500 ppm FA at low temperature of 275 K was significantly higher than that in seawater at higher temperatures, as shown in Table S2 of the supplementary information. Moreover, the pH value determination showed that the pH of the remaining aqueous solution gradually decreased in the process of hydrate formation, showing an increase of dissolved amount of CO_2, as presented in Fig. 13b. The pH values of pure water with FA and seawater with FA indicated that FA possessed buffering capacity, as presented in Fig. 13c and Fig. S13 of the supplementary information. FA could ionize more hydroxyl groups at low temperatures, resulting in an increase in pH, as illustrated in Fig. 13c. The presence of salt ions in the seawater of South China Sea further decreased interfacial tension, as presented in Fig. 13d, which was conductive to CO_2 molecules into aqueous solution though the interface. After more CO_2 molecules were dissolved in the FA aqueous solution, the difference between the mole fraction of CO_2 dissolved in liquid for the equilibrium with liquid CO_2

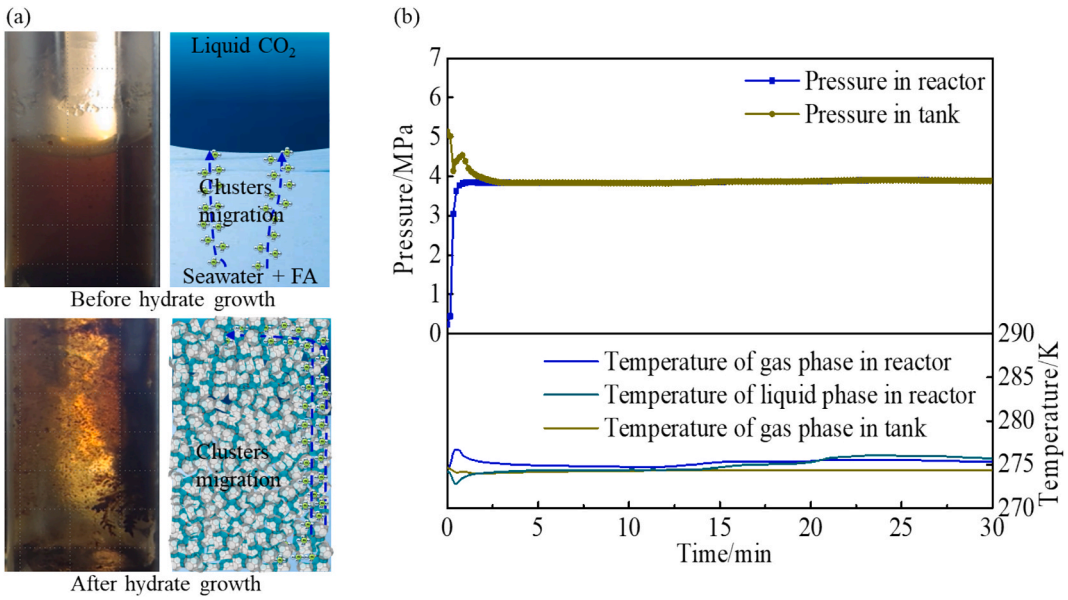

Fig. 12. (a) Morphology before and after CO_2 hydrate formation without temperature difference and (b) Pressure and temperature changes in the process of hydrate formation for the seawater of South China Sea with 500 ppm FA.

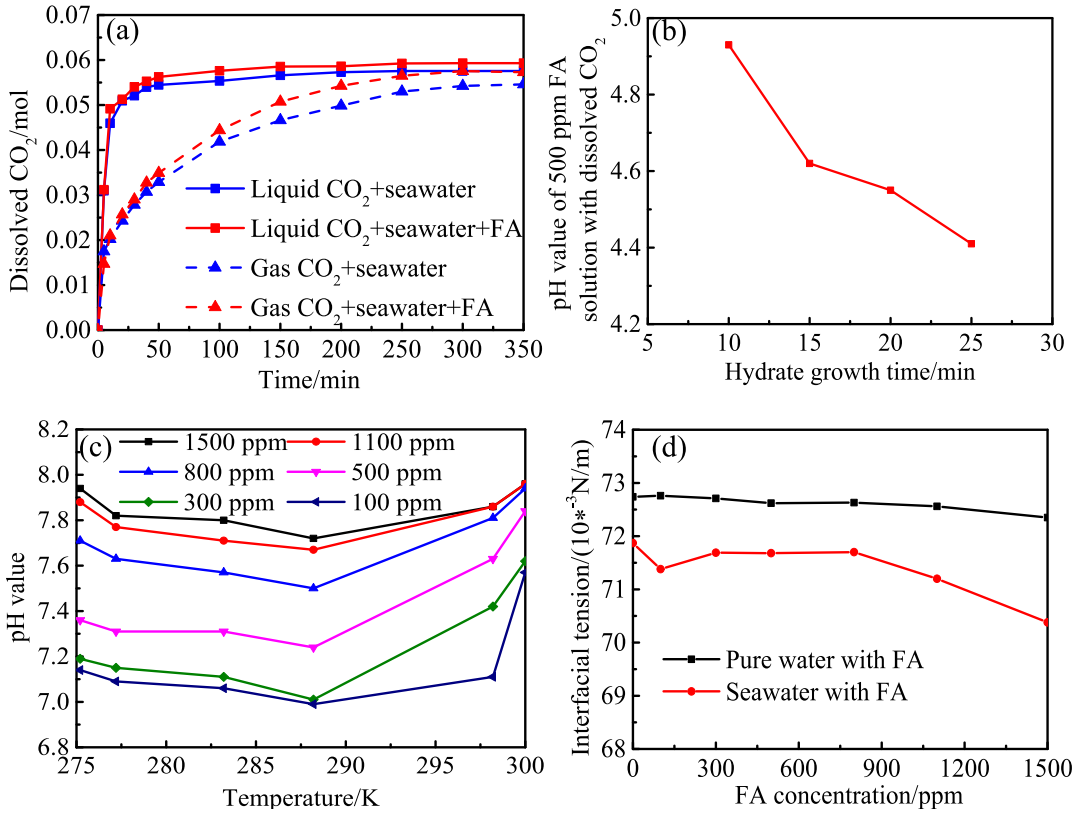

Fig. 13. (a) Moles of dissolved CO_2 in the seawater with 500 ppm FA for liquid CO_2 and gas CO_2 at 284.2 K, (b) pH value changes of remaining FA solution with dissolved CO_2 in the process of CO_2 hydrate growth, (c) pH value changes of aqueous solution with FA in the temperature ranging from 275.2 K to 300.0 K and (d) Interfacial tension changes of pure water and seawater of South China Sea with FA concentration.

and the mole fraction of CO_2 dissolved in liquid for the equilibrium with hydrate became larger in the process of hydrate growth. Δx is considered as the difference between the mole fraction of CO_2 dissolved in liquid for the equilibrium with liquid CO_2 and the mole fraction of CO_2 dissolved in liquid for the equilibrium with hydrate. Therefore, "self-siphoning" phenomenon was easily induced by the mass-transfer driving force and more pronounced at low temperatures. The mass-transfer driving force increased as the temperature decreased, as revealed in Fig. S14 of the supplementary information. The higher the FA concentration, the higher the siphon height of its aqueous solution rose, which might be attributed to mass-transfer driving force to drive FA aqueous solution to enter hydrate pores. Thus, a capillary model was built for in-depth analysis.

The decrease in the contact angle of the FA solution indicated that FA promoted the adsorption of the aqueous solution onto the reactor wall, which in turn facilitated the enhancement of the capillary effect, as shown in Fig. S15 of the supplementary information. A larger mass-transfer driving force was required for the solution to be drawn higher into the hydrate layer, as presented in Fig. S16 of the supplementary information. The height of solution being sucked into the hydrate layer is highly dependent on the strength of interaction between liquid CO_2 and FA aqueous solution due to groups such as carbonyl, carboxyl, hydroxyl and phenol. Some studies have shown that H-bonds, π-bonds, charge transfer complexes and hydrophobic interactions all played an important role in the process of FA clustering into aggregates [84–87]. The FA molecules in aggregates were bridged by water molecules [84,87]. The hydrophobicity of these clusters containing FA is further increased to enhance the affinity between clusters and CO_2 molecules, thereby enhancing the interaction between liquid CO_2 and water molecules to increase the mass-transfer driving force. Carboxyl and phenolic groups of FA, as effective functional groups, coordinated with Na^+, Mg^{2+} and Ca^{2+} ions, which was attributed to the coordination bonds or coordinate covalent bonds formed between the metal ions and FA [88–91]. These metal ions were bridged to FA through water molecules, resulting in the formation of an outer-sphere complex structure. The carboxyl and phenolic groups of FA exerted a synergistic effect in coordinating with metal ions [88]. Ca^{2+} had a better capacity for association due to the smaller charge-to-radius ratio [91]. As a result, FA not only might reduce the concentration of Na^+, Mg^{2+}, and Ca^{2+} ions in the bulk solution during the coordination process, but also remove salt ions from the hydrate surface during hydrate growth. It is the special structure of FA molecules themselves that enables them to strengthen the ability of liquid CO_2 to form hydrate quickly.

In the process of CO_2 hydrate formation for oceanic CO_2 sequestration, it is particularly important to develop environmentally friendly promotors and reduce their dosage to protect the marine ecological environment. The environmental amino acids can be as a good choice, but their dosage is relatively high and the promoting effect of liquid CO_2 to form hydrate is limited. In this work, a low dosage of FA, as one of organic matters in marine sediments, was first selected as a high-efficiency additive. The method proposed in this work makes it possible to use hydrate technology to sequestrate CO_2 on a large scale in ocean areas with water depths of about 400 m, ensuring that the 1 km^2 area can accommodate 119.6 tons of CO_2. Moreover, the annual injection amount of CO_2 will also increase due to rapid CO_2 hydrate formation. For 100,000 tons CO_2 per year of such storage capacity, the capacity can be increased to 100,0000–100,00000 tons CO_2 per year. The cost of oceanic CO_2 sequestration was ranged from $4.7-$12.0 per ton of CO_2, and twice than that of territorial sequestration [92–94]. The average cost of self-sealing oceanic sequestration was $142.0 per ton of CO_2 [95–97]. The hydrate-based CO_2 sequestration was carried out at a depth of 400 m, the cost of sequestration was reduced. Bhati et al [98] also demonstrated that techno-economics of rapid hydrate formation could save the electrical energy requirements. Therefore, the amount of CO_2 sequestration can not only be greatly increased for large-scale projects, but also save a considerable amount of money.

4. Conclusion

This work investigated CO_2 hydrate formation from liquid CO_2 in the presence of FA by morphological observations and the analysis of kinetic experiments. The following conclusions are drawn:

(1) FA has a significant promoting effect on CO_2 hydrate nucleation and growth. The rapid CO_2 hydrate growth within 30.0 min in seawater of the South China Sea was achieved. During the CO_2 hydrate forming process, an interesting "self-siphoning" phenomenon was observed. Aqueous solution was quickly sucked into the hydrate-particles pores and elevated through the pores to the liquid CO_2 phase.

(2) The gas storage capacity of CO_2 hydrate and the hydrate formation rate were 121.8 V/V and 4.11 mmol CO_2/(mol H_2O•min) respectively with 500 ppm FA in a static system. The average conversion rate of water to hydrate for 500 ppm FA was the highest value of 0.038 mol H_2O/(mol H_2O·min), which exhibited an enhancement of 223.5-fold compared to the amino acids in the static system.

(3) The overall hydrate skeleton of CO_2 hydrates by bridging FA remained was stable during CO_2 hydrate dissociation experiment. And the Raman spectroscopy revealed that CO_2 molecules were stably trapped in large cages of CO_2 hydrates.

(4) "Self-siphoning" phenomenon was driven by the mass-transfer driving force due to higher CO_2 solubility in FA aqueous solution. This phenomenon maybe the reason of the rapid formation of hydrates from liquid CO_2.

CRediT authorship contribution statement

Faping Liu: Writing – original draft, Investigation, Data curation, Conceptualization. **Yanhong Wang:** Writing – review & editing, Supervision, Methodology, Funding acquisition. **Xuemei Lang:** Data curation. **Gang Li:** Writing – review & editing. **Shuanshi Fan:** Writing – review & editing, Resources, Project administration, Methodology, Funding acquisition.

Declaration of competing interest

The authors declare that they have no known competing financial interests or personal relationships that could have appeared to influence the work reported in this paper.

Acknowledgments

This work was supported by the Key Research and Development Program of Guangzhou (no. 202206050002) and Special Project for Marine Economy Development of Guangdong (six marine industries) (GDNRC[2024]33).

Data availability

Data will be made available on request.

References

[1] P. Kraaijenbrink, M. Bierkens, A.F. Lutz, W.W. Immerzeel, Impact of a global temperature rise of 15 degrees Celsius on Asia's glaciers, Nature 549 (2017) 257–260.
[2] J.P. Gattuso, A. Magnan, R. Bille, et al., Contrasting futures for ocean and society from different anthropogenic CO_2 emissions scenarios, Science 349 (2015) 1–10.
[3] M. Aminnaji, M.F. Qureshi, H. Dashti, et al., CO_2 gas hydrate for carbon capture and storage applications - Part 1, Energy 300 (2024) 131579.
[4] M. Aminnaji, M.F. Qureshi, H. Dashti, et al., CO_2 gas hydrate for carbon capture and storage applications - Part 2, Energy 300 (2024) 131580.
[5] M. Bui, C.S. Adjiman, A. Bardow, et al., Carbon capture and storage (CCS): the way forward, Energy Environ. Sci. 11 (2018) 1062–1176.
[6] Y.S. Yu, X.W. Zhang, J.W. Liu, Y. Lee, X.S. Li, Natural gas hydrate resources and hydrate technologies: A review and analysis of the associated energy and global warming challenges, Energy Environ. Sci. 14 (2021) 5611–5668.
[7] Y.H. Teng, D.X. Zhang, Long-term viability of carbon sequestration in deep-sea sediments, Sci. Adv. 4 (2018) eaao6588.
[8] Y. Ge, L. Wang, Y.C. Song, Large-scale experimental study on marine hydrate-based CO_2 sequestration, Energy 312 (2024) 133649.
[9] J.J. Zheng, Z.R. Chong, M.F. Qureshi, P. Linga, Carbon dioxide sequestration via gas hydrates: A potential pathway toward decarbonization, Energy Fuels 34 (2020) 10529–10546.
[10] K.Z. House, D.P. Schrag, C.F. Harvey, K.S. Lackner, Permanent carbon dioxide storage in deep-sea sediments, Appl. Phys. Sci. 103 (2006) 12291–12295.
[11] V. Dhamu, X. Mengqi, M.F. Qureshi, Z.Y. Yin, A.K. Jana, P. Linga, Evaluating CO_2 hydrate kinetics in multi-layered sediments using experimental and machine learning approach: applicable to CO_2 sequestration, Energy 290 (2024) 129947.
[12] F. Qanbaria, M. Pooladi-Darvish, S.H. Tabatabaie, S. Geramid, Storage of CO_2 as hydrate beneath the ocean floor, Energy Procedia 4 (2011) 3997–4004.
[13] P.G. Brewer, G. Friederich, E.T. Peltzer, F.M. Orr, Direct experiments on the ocean disposal of fossil fuel CO_2, Science 284 (1999) 943.

[14] G. Vishwakarma, V. Dhamu, M.F. Qureshi, G. Bhattacharjee, T. Pradeep, P. Linga, Understanding the kinetics of CO_2 hydrate formation in dry water for carbon capture and storage: X-ray diffraction and in situ raman studies, ACS Appl. Mater. Interfaces 17 (2025) 4865–4874.

[15] V. Dhamu, M. Xiao, M.F. Qureshi, P. Linga, Deciphering the CO_2 hydrates formation dynamics in brine-saturated oceanic sediments using experimental and machine learning modelling approach, Energy 31 (2024) 133802.

[16] Y. Guo, S.X. Li, H. Sun, D.D. Wu, L. Liu, N.T. Zhang, X.W. Qin, C. Lu, Enhancing gas production and CO_2 sequestration from marine hydrate reservoirs through optimized CO_2 hydrate cap, Energy 303 (2024) 131821.

[17] M.J. Yang, M.Y. Wu, Z.M. Yang, P.F. Wang, B.B. Chen, Y.C. Song, Behaviors of hydrate cap formation via CO_2-H_2O collaborative injection: Applying to secure marine carbon storage, Gas Sci. Eng. 131 (2024) 205451.

[18] L. Yang, P. Gao, Y.Q. Xia, W.X. Pang, Q.P. Li, L.X. Zhang, J.F. Zhao, Y.C. Song, Enhancing carbon sequestration efficiency and safety through albumin-optimized CO_2 hydrate distribution and geological layer stability: An innovative approach, Energy 305 (2024) 132276.

[19] S.H. Ma, X. Tian, Z.X. Liu, Z.R. Wu, G.J. Li, X.M. Guan, J.N. Zheng, M.J. Yang, Formation and decomposition characteristics of CO_2+TBAB hydrate for a safer CO_2 storage, Energy 307 (2024) 132801.

[20] G.J. Zhao, M.J. Yang, W.X. Pang, G.J. Gong, J.N. Zheng, P. Zhang, B.B. Chen, Effects of hydrate cap on leakage prevention and capacity improvement of sub-seabed CO_2 sequestration, Chem. Eng. J. 450 (2022) 138493.

[21] G.J. Zhao, J.N. Zheng, G.J. Gong, B.B. Chen, M.J. Yang, Y.C. Song, Formation characteristics and leakage termination effects of CO_2 hydrate cap in case of geological sequestration leakage, Appl. Energy 351 (2023) 121896.

[22] H.R. Sun, J. Chen, X. Ji, G. Karunakaran, B.B. Chen, P.G. Ranjith, Y.C. Song, M. J. Yang, Optimizing CO_2 hydrate storage: dynamics and stability of hydrate caps in submarine sediments, Appl. Energy 376 (2024) 124309.

[23] Y.Q. Xia, T. Yu, L. Yang, B.B. Chen, L.L. Jiang, M.J. Yang, Y.C. Song, Multi-state CO_2 distribution patterns for subsea carbon sequestration assisted by large-scale CO_2 hydrate caps, Energy 320 (2025) 135231.

[24] M.Y. Wu, H.R. Sun, Q.B. Liu, X. Lv, B.B. Chen, M.J. Yang, Y.C. Song, Enhancing CO_2 sequestration safety with hydrate caps: A comparative study of CO_2 injection modes and saturation effects, Energy 320 (2025) 135044.

[25] J.Z. Chen, S.H. Mei, Gas-saturated carbon dioxide hydrates above sub-seabed carbon sequestration site and the formation of self-sealing cap, Gas Sci. Eng. 111 (2023) 204913.

[26] Y.H. Gu, X.J. Liu, Y. Li, H.F. Lu, C.L. Xu, J.F. Ren, G.J. Chen, P. Linga, J.Z. Zhao, Z. Y. Yin, Feasibility analysis of liquid CO_2 injection and sequestration as hydrates in South China Sea marine sediments over 100 years, Appl. Energy 38 (2025) 125068.

[27] H.Y. Ye, Y.X. Yao, D.Y. Chen, J.Y. Chen, X.Z. Wu, D.Y. Li, M.C. Zi, How shallow CO_2 hydrate cap affects depressurization production in deeper natural gas hydrate reservoirs: An example at Site W17, South China Sea, J. Clean. Prod. 478 (2024) 143954.

[28] Y. Tabe, S. Hirai, K. Okazaki, Measurement of clathrate-hydrate film thickness formed at the interface between liquid CO_2 and water, Greenhouse Gas Control Technol. (1999) 311–315.

[29] Y. Tabe, S. Hirai, K. Okazaki, Measurement of CO_2 hydrate film thickness based on mass transport mechanism, J. Chem. Eng. Jpn. 33 (2000) 612–616.

[30] T. Uchida, J. Kawabata, Measurements of mechanical properties of the liquid CO_2-water-CO_2-hydrate system, Energy 22 (1997) 357–361.

[31] Y. Nakajima, H. Shirota, S. Namie, Observation of CO_2 hydrate formation in high pressured water, Proceedings of the Thirteenth International Offshore and Polar Engineering Conference 1 (2003) 317-320.

[32] Y.J. Zhu, Y. Zhang, Y.Z. Chen, Y. Xie, J.R. Zhong, X.H. Wang, P. Xiao, Y.F. Sun, C. Y. Sun, G.J. Chen, The morphology of liquid CO_2 hydrate films at different temperatures under saturation pressure, Chem. Eng. J. 497 (2024) 154478.

[33] M.L. Wang, Y.F. Sun, W.X. Pang, Q.P. Li, T. Huang, H.N. Chen, M. Wang, J. R. Zhong, L.L. Ren, D. Rao, B. Liu, C.Y. Sun, G.J. Chen, Enhanced hydrate formation at the liquid CO_2-brine interface with shear flow for solid CO_2 sequestration, Gas Sci. Eng. 130 (2024) 205433.

[34] X.J. Liu, J.D. Zhang, Y.H. Gu, H.L. Huang, Y. Li, J.Y. Sun, H.F. Lu, C.L. Xu, J.F. Ren, Z.Y. Yin, Investigation on liquid CO_2 forming CO_2 hydrates in sands: A kinetic study with implication on hydrate-based CO_2 sequestration, Chem. Eng. J. 505 (2025) 159179.

[35] J.W. Lee, M.K. Chun, K.M. Lee, Y.J. Kim, H. Lee, Phase equilibria and kinetic behavior of CO_2 hydrate in electrolyte and porous media solutions: Application to ocean sequestration of CO_2, Korean J. Chem. Eng. 19 (2002) 673–678.

[36] R.B. Lamorena, W. Lee, Formation of carbon dioxide hydrate in soil and soil mineral suspensions with electrolytes, Environ. Sci. Technol. 42 (2008) 2753–2759.

[37] S.Y. Zeng, Z.Y. Yin, J.J. Ren, D.R. Bhawangirkar, L. Huang, P. Linga, Effect of $MgCl_2$ on CO_2 sequestration as hydrates in marine environment: A thermodynamic and kinetic investigation with morphology insights, Energy 286 (2024) 129616.

[38] V. Dhamu, M.F. Qureshi, N. Selvaraj, L.J. Yuanmin, I.T. Guo, P. Linga, Dual promotional effect of L-tryptophan and 1,3-dioxane on CO_2 hydrate kinetics in seawater under static/unstatic conditions for carbon capture and storage application, Energy Fuels 38 (2024) 11980–11993.

[39] K. Jeenmuang, P. Pornaroontham, M.F. Qureshi, P. Linga, P. Rangsunvigit, Micro kinetic analysis of the CO_2 hydrate formation and dissociation with L-tryptophan in brine via high pressure in situ Raman spectroscopy for CO_2 sequestration, Chem. Eng. J. 479 (2024) 147691.

[40] M.F. Qureshi, M. Khraisheh, F. AlMomani, Experimentally measured methane hydrate phase equilibria and ionic liquids inhibition performance in Qatar's seawater, Sci. Rep. 10 (2020) 19463.

[41] M.F. Qureshi, J.J. Zheng, H. Khandelwal, P. Venkataraman, A. Usadi, T. A. Barckholtz, A.B. Mhadeshwar, P. Linga, Laboratory demonstration of the stability of CO_2 hydrates in deep-oceanic sediments, Chem. Eng. J. 432 (2022) 134290.

[42] M.F. Qureshi, H. Khandelwal, A. Usadi, T.A. Barckholtz, A.B. Mhadeshwar, P. Linga, CO_2 hydrate stability in oceanic sediments under brine conditions, Energy 256 (2022) 124625.

[43] J. Gauteplass, S. Almenningen, G. Ersland, T. Barth, Hydrate seal formation during laboratory CO_2 injection in a cold aquifer, Int. J. Greenh. Gas Control. 78 (2018) 21–26.

[44] P. Babu, S. Datta, R. Kumar, P. Linga, Impact of experimental pressure and temperature on semiclathrate hydrate formation for pre-combustion capture of CO_2 using tetra-n-butyl ammonium nitrate, Energy 78 (2014) 458–464.

[45] H.P. Veluswamy, A. Kumar, K. Premasinghe, P. Linga, Effect of guest gas on the mixed tetrahydrofuran hydrate kinetics in a quiescent system, Appl. Energy 207 (2017) 573–583.

[46] X.B. Zhou, Z. Long, C.P. Tang, D.Q. Liang, Kinetic measurements on CO_2 hydrate formation in the presence of tetra-n-butyl ammonium bromide, Energy Fuels 32 (2018) 9683–9691.

[47] N.N. Nguyen, A.V. Nguyen, K.T. Nguyen, L. Rintoul, L.X. Dang, Unexpected inhibition of CO_2 gas hydrate formation in dilute TBAB solutions and the critical role of interfacial water structure, Fuel 185 (2016) 517–523.

[48] A. Mohammadi, M. Manteghian, A. Haghtalab, A.H. Mohammadi, M. Rahmati-Abkenar, Kinetic study of carbon dioxide hydrate formation in presence of silver nanoparticles and SDS, Chem. Eng. J. 237 (2014) 387–395.

[49] C.F.D. Lirio, F.L.P. Pessoa, A.M.C. Uller, Storage capacity of carbon dioxide hydrates in the presence of sodium dodecyl sulfate (SDS) and tetrahydrofuran (THF), Chem. Eng. Sci. 96 (2013) 118–123.

[50] B. ZareNezhad, V. Montazeri, Development of a high efficient gas to hydrate (GTH) conversion process using SDS kinetic promoter for maximizing the CO_2 recovery with minimum energy consumption, Energ. Convers, Manage 79 (2014) 289–293.

[51] S.R. Firoozabadi, M. Bonyadi, A comparative study on the effects of Fe_3O_4 nanofluid, SDS and CTAB aqueous solutions on the CO_2 hydrate formation, J. Mol. Liq. 300 (2020) 112251.

[52] J.H. Sa, G.H. Kwak, K. Han, D. Ahn, K.H. Lee, Gas hydrate inhibition by perturbation of liquid water structure, Sci Rep-Uk 5 (2015) 11526.

[53] P.S.R. Prasad, B.S. Kiran, Are the amino acids thermodynamic inhibitors or kinetic promoters for carbon dioxide hydrates? J. Nat. Gas Sci. Eng. 52 (2018) 461–466.

[54] J.H. Sa, G.H. Kwak, B.R. Lee, D.H. Park, K. Han, K.H. Lee, Hydrophobic amino acids as a new class of kinetic inhibitors for gas hydrate formation, Sci Rep-Uk 3 (2013) 2428.

[55] W.X. Wang, C. Ma, P.Z. Lin, L.Y. Sunc, A.I. Cooper, Gas storage in renewable bioclathrates, Energy Environ. Sci. 6 (2013) 105–107.

[56] Y.C. Song, S.J. Wang, Z.C. Cheng, M.X. Huang, Y. Zhang, J.N. Zheng, L.L. Jiang, Y. Liu, Dependence of the hydrate-based CO_2 storage process on the hydrate reservoir environment in high-efficiency storage methods, Chem. Eng. J. 415 (2021) 128937.

[57] M.F. Qureshi, V. Dhamu, A. Usadi, T.A. Barckholtz, A.B. Mhadeshwar, P. Linga, CO_2 hydrate formation kinetics and morphology observations using high-pressure liquid CO_2 applicable to sequestration, Energy Fuels 36 (2022) 10627–10641.

[58] V. Dhamu, M.F. Qureshi, M.A. Barckholtz, A.B. Mhadeshwar, P. Linga, Evaluating liquid CO_2 hydrate formation kinetics, morphology, and stability in oceanic sediments on a lab scale using top injection, Chem. Eng. J. 478 (2023) 147200.

[59] V. Dhamu, M.F. Qureshi, S. Abubakar, A. Usadi, T.A. Barckholtz, A.B. Mhadeshwar, P. Linga, Investigating high-pressure liquid CO_2 hydrate formation, dissociation kinetics, and morphology in brine and freshwater static systems, Energy Fuels 37 (2023) 8406–8420.

[60] N. Li, J.Y. Kan, C.Y. Sun, G.J. Chen, Hydrate formation from liquid CO_2 in a glass beads bed, Chinese, J. Chem. Eng. 43 (2022) 185–191.

[61] L.X. Zhang, Y.M. Kuang, S. Dai, J.Q. Wang, J.F. Zhao, Y.C. Song, Kinetic enhancement of capturing and storing greenhouse gas and volatile organic compound: Micro-mechanism and micro-structure of hydrate growth, Chem. Eng. J. 379 (2020) 122357.

[62] R.B. Lamorena, D. Kyung, W. Lee, Effect of organic matters on CO_2 hydrate formation in ulleung basin sediment suspensions, Environ. Sci. Technol. 45 (2011) 6196–6203.

[63] Y.Z. Liu, L.X. Zhang, L. Yang, H.S. Dong, J.F. Zhao, Y.C. Song, Behaviors of CO_2 hydrate formation in the presence of acid-dissolvable organic matters, Environ. Sci. Technol. 55 (2021) 6206–6213.

[64] S.Q. Hu, M.J. Wang, P. Wang, H. Jiang, M. Cheng, S.Q. Sun, C.L. Li, Self-repairing coating with excellent mechanical properties by compatibility epoxy resin-loaded polyurea formaldehyde microcapsule, Adv. Eng. Mater. 25 (2023) 2201668.

[65] C.X. Li, H.Y. Dai, C. Gao, L. Jiang, Bioinspired inner microstructured tube controlled capillary rise, PNAS 116 (2019) 12705.

[66] S.W. Wu, S.Y. Tian, R.D. Jian, T.N. Wu, T.F. Luo, G.P. Xiong, Graphene petal foams with hierarchical micro- and nano-channels for ultrafast spontaneous and continuous oil recovery, J. Mater. Chem. A 10 (2022) 11651–11658.

[67] N. Akhras, G. Singh, K.K. Gill, S. Bola, K. Al-Hakeem, N.M. Reis, Numerical modeling and experimental validation of fluid flow in micro and meso-fluidic siphons, Front. Chem. Eng. 6 (2024) 1443949.

[68] N.N. Cao, S.T. Lu, Y. Yao, C.X. Liu, P. Zhang, Q.Y. Xiong, Y. Li, X.H. Wu, High-rate long-lasting solar desalination towards hypersaline brine enabled by introducing a siphon-drop mode, Chem. Eng. J. 430 (2022) 133043.

[69] Y.F. Zhang, L.P. Yang, J.H. Li, W.W. Zhao, Y.X. Liu, M. Ding, G.B. Xue, Thermal distillation of hypersaline waters toward zero liquid discharge via spontaneously siphon-channeling crystallized salt, Chem. Eng. J. 498 (2024) 155095.

[70] X.L. Zhang, Y. Dong, Z. He, H.Y. Gong, X. Xu, M.Y. Zhao, H.L. Qin, Efficient gas transportation using bioinspired superhydrophobic yarn as the gas-siphon underwater, ACS Appl. Mater. Interfaces 12 (2020) 18174–18181.
[71] M. Ricaurte, T. Jean-Philippe, A. Asbai, Experimental data, modeling, and correlation of carbon dioxide solubility in aqueous solutions containing low concentrations of clathrate hydrate promoters: Application to CO_2-CH_4 gas mixtures, Ind. Eng. Chem. Res. 51 (2012) 3157–3169.
[72] M. Mohammadi, A. Haghtalab, Z. Fakhroueian, Experimental study and thermodynamic modeling of CO_2 gas hydrate formation in presence of zinc oxide nanoparticles, J. Chem. Thermodyn. 96 (2016) 24–33.
[73] J.B. Klauda, S.I. Sandler, A fugacity model for gas hydrate phase equilibria, Ind. Eng. Chem. Res. 39 (2000) 3377–3386.
[74] M.O. Gborigi, D.A. Riestenberg, M.J. Lance, S.D. McCallum, Y. Atallah, C. Tsouris, Raman spectroscopy of a hydrated CO_2/water composite, J. Petroleum Sci. Eng. 56 (2007) 65–74.
[75] L.Z. Chen, H.L. Lu, J.A. Ripmeester, Raman spectroscopic study of CO_2 in hydrate cages, Chem. Eng. Sci. 138 (2015) 706–711.
[76] X.J. Liu, J.J. Ren, D.Y. Chen, Z.Y. Yin, Comparison of SDS and L-Methionine in promoting CO_2 hydrate kinetics: Implication for hydrate-based CO_2 storage, Chem. Eng. J. 438 (2022) 135504.
[77] X.J. Liu, Y. Li, G.J. Chen, D.Y. Chen, B. Sun, Z.Y. Yin, Coupling amino acid with THF for the synergistic promotion of CO_2 hydrate micro kinetics: Implication for hydrate-based CO_2 sequestration, ACS Sustainable Chem. Eng. 11 (2023) 6057–6069.
[78] E. Pagar, S.K. Burla, V. Kumar, H.P. Veluswamy, Influence of amino acids on gas hydrate formation and dissociation kinetics using flue gas (CO_2 + N_2 mixture) in silica sand under saline/non-saline conditions for CO_2 sequestration, Appl. Energy 367 (2024) 123460.
[79] G. Bhattacharjee, M.N. Goh, S.E.K. Arumuganainar, E. Zhang, P. Linga, Ultra-rapid uptake and the highly stable storage of methane as combustible ice, Energy Environ. Sci. 13 (2020) 4946–4961.
[80] Y. Zhang, J. Zhao, G. Bhattacharjee, H.Z. Xu, M.J. Yang, R. Kumar, P. Linga, Synthesis of methane hydrate at ambient temperature with ultra-rapid formation and high gas storage capacity, Energy Environ. Sci. 15 (2022) 5362–5378.
[81] H.L. Huang, X.J. Liu, H.F. Lu, C.L. Xu, J.Z. Zhao, Y. Li, Y.H. Gu, Z.Y. Yin, Introducing sodium lignosulfonate as an effective promoter for CO_2 sequestration as hydrates targeting gaseous and liquid CO_2, Adv. Appl. Energy 14 (2024) 100175.
[82] F.P. Liu, Y.H. Wang, X.M. Lang, G. Li, S.S. Fan, Hydrate formation and dissociation of liquid CO_2 with seawater containing organic matters in sand, Energy Fuels 38 (2024) 17750–17760.
[83] S.F. Li, S.S. Fan, J.Q. Wang, X.M. Lang, Y.H. Wang, Semiclathrate hydrate phase equilibria for CO_2 in the presence of tetra-n-butyl ammonium halide (bromide, chloride, or fluoride), J. Chem. Eng. Data 55 (2010) 3212–3215.
[84] A. Porquet, L. Bianchi, S. Stoll, Molecular dynamic simulations of fulvic acid clusters in water, Colloid Surface A 217 (2003) 49–54.
[85] R.L. Wershaw, Molecular aggregation of humic substances, Soil Sci. 164 (1999) 803–813.
[86] C.E. Clapp, M.H.B. Hayes, Sizes and shapes of humic substances, Soil Sci. 164 (1999) 777–789.
[87] R.C. Averett, J.A. Leenheer, D.M. Mac Knight, K.A. Thorn, Humic substances in the Suwannee river, Georgia: interactions, properties, and proposed structures, Water Supply Paper (1994) 2373.
[88] J. Adusei-Gyamfi, B. Ouddane, L. Rietveld, J.P. Cornard, J. Criquet, Natural organic matter-cations complexation and its impact on water treatment: A critical review, Water Res. 160 (2019) 130–147.
[89] E. Iskrenova-Tchoukova, A.G. Kalinichev, R.J. Kirkpatrick, Metal cation complexation with natural organic matter in aqueous solutions: Molecular dynamics simulations and potentials of mean force, Langmuir 26 (2010) 15909–15919.
[90] M. Fizer, V. Sidey, S. Milyovich, O. Fizer, A DFT study of fulvic acid binding with bivalent metals: Cd, Cu, Mg, Ni, Pb, Zn, J. Mol. Graph. Model. 102 (2021) 107800.
[91] A.J.A. Aquino, D. Tunega, G.E. Schaumann, G. Haberhauer, M.H. Gerzabek, H. Lischka, The functionality of cation bridges for binding polar groups in soil aggregates, Int. J. Quantum Chem. 111 (2011) 1531–1542.
[92] E. Kintisch, Underground injections turn carbon dioxide to stone, Science (2016).
[93] X.Y. Xu, Q. Li, B.F. Cai, G.Z. Liu, L.Y. Pang, M. Jing, J. Guo, Cost assessment and potential evaluation of geologic carbon storage in China based on least-cost path analysis, Appl. Energy 371 (2024) 123622.
[94] C. Hendriks, W. Graus, F. van Bergen, Global carbon dioxide storage potential and costs, Report No. EEP-02001. Ecofys, Utrecht, 2004.
[95] J.K. Eccles, L. Pratson, Economic evaluation of offshore storage potential in the US exclusive economic zone, Greenh. Gases, Sci. Technol. 3 (2013) 84–95.
[96] Y. Kumar, J.S. Sangwai, Environmentally sustainable large-scale CO_2 sequestration through hydrates in offshore basins: ab initio comprehensive analysis of subsea parameters and economic perspective, Energy Fuels 37 (2023) 8739–8764.
[97] L. Amado, Reservoir Exploration and Appraisal, Elsevier, 2013.
[98] A. Bhati, M. Hamalian, V. Bahadur, Techno-economic modeling of carbon dioxide hydrate formation for carbon sequestration, Appl. Energy 377 (2025) 124491.